Hemodynamics regulate spatiotemporal artery muscularization in the developing circle of Willis

Siyuan Cheng[1,2,3#], Ivan Fan Xia[1,2,3#], Renate Wanner[1,2,3], Javier Abello[4], Amber N. Stratman[4], and Stefania Nicoli[1,2,3*]

[1]Department of Genetics, Yale School of Medicine, 333 Cedar St, New Haven, CT 06520, USA

[2]Yale Cardiovascular Research Center, Section of Cardiology, Department of Internal Medicine, Yale School of Medicine, 300 George St, New Haven, CT 06511, USA

[3]Vascular Biology & Therapeutics Program, Yale School of Medicine, 10 Amistad St, New Haven, CT 06520, USA

[4]Department of Cell Biology & Physiology, School of Medicine, Washington University in St. Louis, 660 S. Euclid Ave, St. Louis, MO 63110, USA

[#] These authors contributed equally

[*] Correspondence to: stefania.nicoli@yale.edu

Abstract

Vascular smooth muscle cells (VSMCs) envelop vertebrate brain arteries, playing a crucial role in regulating cerebral blood flow and neurovascular coupling. The dedifferentiation of VSMCs is implicated in cerebrovascular diseases and neurodegeneration. Despite its importance, the process of VSMC differentiation on brain arteries during development remains inadequately characterized. Understanding this process could aid in reprogramming and regenerating differentiated VSMCs in cerebrovascular diseases. In this study, we investigated VSMC differentiation on the zebrafish circle of Willis (CoW), comprising major arteries that supply blood to the vertebrate brain. We observed that the arterial expression of CoW endothelial cells (ECs) occurs after their migration from the cranial venous plexus to form CoW arteries. Subsequently, acta2+ VSMCs differentiate from pdgfrb+ mural cell progenitors upon recruitment to CoW arteries. The progression of VSMC differentiation exhibits a spatiotemporal pattern, advancing from anterior to posterior CoW arteries. Analysis of blood flow suggests that earlier VSMC differentiation in anterior CoW arteries correlates with higher red blood cell velocity wall shear stress. Furthermore, pulsatile blood flow is

required for differentiation of human brain pdgfrb+ mural cells into VSMCs as well as VSMC differentiation on zebrafish CoW arteries. Consistently, the flow-responsive transcription factor klf2a is activated in ECs of CoW arteries prior to VSMC differentiation, and *klf2a* knockdown delays VSMC differentiation on anterior CoW arteries. In summary, our findings highlight the role of blood flow activation of endothelial klf2a as a mechanism regulating the initial VSMC differentiation on vertebrate brain arteries.

Introduction

Vascular smooth muscle cells (VSMCs) are contractile mural cells wrapping around endothelial cells (ECs) of large vessels, especially arteries (Ando et al., 2022; Donadon & Santoro, 2021; Stratman et al., 2020). The expression of contractile proteins, such as alpha-smooth muscle actin (encoded by *acta2*), distinguishes VSMCs from pericytes, the other type of mural cells primarily associated with small vessels (Bahrami & Childs, 2020; Donadon & Santoro, 2021; Stratman et al., 2020). VSMCs are important for arterial homeostasis (Basatemur, Jorgensen, Clarke, Bennett, & Mallat, 2019). In the brain, VSMC constriction and relaxation is essential for functional hyperemia in neurovascular coupling (Hill et al., 2015; Kaplan, Chow, & Gu, 2020). Phenotype switching or dedifferentiation of VSMCs, marked by lower expression of contractile proteins, is prominent in pathological progression of atherosclerosis (Basatemur et al., 2019). VSMC phenotype switching or dedifferentiation also contributes to cerebrovascular diseases and neurodegeneration (Aguilar-Pineda et al., 2021; Chou et al., 2022; Frosen & Joutel, 2018; Milewicz et al., 2010; Oka et al., 2020; Poittevin et al., 2014). As development and regeneration share many common molecular and cellular mechanisms (Nowotarski & Sánchez Alvarado, 2016), insights on VSMC differentiation on brain arteries during development may inform strategies to reprogram and regenerate dedifferentiated VSMCs and alleviate cerebrovascular diseases.

VSMCs differentiate from heterogenous perivascular progenitors of mesoderm and neural crest origins (Ando et al., 2019; Donadon & Santoro, 2021; Whitesell et al., 2019). Previous research described various mechanisms that regulate VSMC differentiation. Autonomous Notch activation is required for specification of *pdgfrb*+ mural cell progenitors from peri-arterial mesenchyme, and these progenitors later differentiate into *acta2*+ VSMCs (Ando et al., 2019). Arterial Notch signaling activated by blood flow is necessary for *acta2*+ VSMC emergence on zebrafish trunk dorsal aorta (X. Chen, Gays, Milia, & Santoro, 2017). Chemokine signaling promotes VSMC association with zebrafish dorsal aorta, whereas blood flow responsive transcription factor krüppel-like factor 2 (encoded by *klf2a* in zebrafish) prevents their association with the adjacent cardinal vein (Stratman et al., 2020). Endothelial BMP signaling and autonomous *foxc1* expression regulate VSMC differentiation in zebrafish ventral head (Watterston, Zeng, Onabadejo, & Childs, 2019; Whitesell et al., 2019). Autonomous expression of an ATP-sensitive potassium channel modulates VSMC differentiation from *pdgfrb*+ progenitors in the brain (Ando et al., 2022). These studies suggest that VSMC differentiation is highly organotypic.

The circle of Willis (CoW) consists of major arteries that supply blood to the vertebrate brain, including internal carotid arteries (ICAs) and posterior communicating arteries (PCAs) (Campbell et al., 2019; Schröder, Moser, & Huggenberger, 2020). In early development, ICAs are the first large arteries to form and supply all circulation in the developing brain (Kathuria, Gregg, Chen, & Gandhi, 2011; Menshawi, Mohr, & Gutierrez, 2015). In adults, posterior circulation becomes independent, and ICAs remain major feeding arteries in anterior, while connected to posterior circulation with PCAs, completing a circle of arteries (Kathuria et al., 2011; Schröder et al., 2020). In adults, intracranial aneurysms are frequently found close to CoW arteries (Frosen & Joutel, 2018). CoW arteries are wrapped by VSMCs, and VSMC dedifferentiation and hyperplasia are described in carotid atherosclerosis and Moyamoya disease (Chou et al., 2022; Fox, Dorschel, Lawton, & Wanebo, 2021). Spatiotemporal dynamics of VSMC differentiation on vertebrate CoW arteries during development have not been thoroughly investigated. VSMC differentiation is difficult to observe *in vivo* with mammalian models, as mammalian embryos develop in utero and depend on maternal circulation. Zebrafish

is an important vertebrate model for vascular development, as zebrafish embryos are externally fertilized, optically clear, and thus accessible to confocal live imaging of developing blood vessels (Stratman & Weinstein, 2021). Establishment of zebrafish fluorescent transgenic reporter lines with *pdgfrb* and *acta2* promoters enables *in vivo* visualization and assessment of mural cells and VSMCs (Ando et al., 2016; Whitesell et al., 2014). In addition, zebrafish CoW shows comparable geometry to human CoW: the caudal division of the internal carotid artery (CaDI) in zebrafish is comparable to human ICA, and the posterior communicating segment (PCS) in zebrafish is comparable to human PCA (Isogai, Horiguchi, & Weinstein, 2001). Taking advantage of the zebrafish model, we describe the spatiotemporal pattern of VSMC differentiation on CoW arteries, and associate this pattern with blood flow activation of *klf2a* in arterial ECs.

Zebrafish COW vessel nomenclature	
CaDI	Caudal division of the internal carotid artery
BCA	Basal communicating artery
PCS	Posterior communicating segment

Results

Artery muscularization is spatiotemporally regulated in CoW arteries

In zebrafish brain, arteries are formed by ECs from cranial venous plexus (Fujita et al., 2011). Recent single-cell transcriptome profiling of vascular cells in prenatal human brain also supports an endothelial differentiation trajectory from proliferative venous ECs to quiescent arterial ECs (Crouch et al., 2022). To establish the temporal sequence of CoW arterial specification and VSMC differentiation, we started with confocal live imaging of fluorescent transgenic reporter lines Tg(*flt4:yfp*)^{hu4881}, which labels primitive venous ECs, and Tg(*kdrl:hras-mcherry*)^{s896}, which is expressed in all ECs but enriched in arterial ECs, at four stages starting at 32 hours post fertilization (hpf), when CoW arteries are assembled (Chi et al., 2008; Hogan et al., 2009; Isogai et

al., 2001). As arterial ECs express higher *kdrl*, we used the intensity of *mcherry* as an indicator of artery specification (Figure 1A-1E) (Chi et al., 2008). We found that when ECs from cranial venous plexus migrated to form CoW arteries at 32 hpf, they still retained primitive venous identity, as indicated by *flt4* expression (Figure 1A). When connections between cranial venous plexus and CoW arteries disappeared at 54 hpf, CoW arteries no longer expressed primitive venous *flt4* (Figure 1B). Expression of arterial enriched *kdrl* in CaDI and PCS at 3 days post fertilization (dpf) was significantly higher than 32 hpf (Figure 1C and 1E). At 4 dpf, *kdrl* expression in CoW arteries remained comparable to 3 dpf, suggesting that arterial specification of CoW was completed by 3 dpf (Figure 1C-1E). Together, these data suggest CoW morphogenesis precedes arterial endothelial gene expression.

Previous research suggested that *acta2*+ VSMCs on CoW arteries differentiate from *pdgfrb*+ mural cell progenitors (Ando et al., 2022; Ando et al., 2019). Thus, to characterize spatiotemporal dynamics of VSMC differentiation on CoW arteries, we performed confocal live imaging of Tg(*acta2:mcherry*)^{ca8}, TgBAC(*pdgfrb:egfp*)^{ncv22}, and Tg(*kdrl:cerulean*)^{sd24}, to visualize respectively VSMCs (red), *pdgfrb*+ progenitors (green), and developing arteries (white) at four stages starting from 32 hpf (Figure 2) (Ando et al., 2016; Page et al., 2013; Whitesell et al., 2014). We found that *pdgfrb*+ progenitors emerged on CoW arteries around 54 hpf after CoW morphogenesis, and most *pdgfrb*+ progenitors did not express *acta2* at 54 hpf (Figure 2A-2B, 2E-2F, and S1A-S1B). The number of *pdgfrb*+ progenitors on CoW arteries increased temporally from 54 hpf to 3 dpf (Figure 2B, 2C, and 2E). Notably, while many *pdgfrb*+ cells on CaDI differentiated into *acta2*+ VSMCs by 3 dpf, *acta2*+ VSMCs were hardly observed on adjacent BCA or PCS, suggesting that VSMC differentiation started between 54 hpf and 3 dpf on CaDI but not BCA or PCS (Figure 2B-2C, 2E-2F, and S1A-S1B). At 4 dpf, the number of *pdgfrb*+ cells on CoW arteries remained comparable to 3 dpf, while the number of *acta2*+ VSMCs on CaDI increased (Figure 2C-2F and S1A-S1B). Importantly, most *pdgfrb*+ cells on BCA and PCS only started to express *acta2* around 4 dpf, much later than CaDI (Figure 2C-2F and S1A-S1B). These findings support that differentiation of acta2+ VSMCs from pdgfrb+ progenitors progresses spatially and temporally along the anterior to posterior direction in CoW arteries.

CoW arteries have spatiotemporal difference in hemodynamics

Our data suggest that VSMCs on CaDI of anterior CoW differentiate much earlier than BCA and PCS of posterior CoW, although all *acta2*+ VSMCs on CoW differentiated from *pdgfrb*+ progenitors after they were recruited to CoW (Figure 2 and S1). In addition, anterior and posterior CoW vascular morphogenesis and arterial specification occurred around the same time (Figure 1). We speculate that hemodynamic distribution may contribute to the spatiotemporal difference in VSMC differentiation on CoW arteries. CaDI receive proximal arterial feed through lateral dorsal aorta from cardiac outflow tract (Isogai et al., 2001). Furthermore, CaDI differs from the BCA or PCS in terms of overall vascular geometry, which is among determinants of local vascular hemodynamic forces such as wall shear stress (WSS) (Katritsis et al., 2007). To explore this possibility, we performed microangiography with a high molecular weight fluorescent dextran to determine each CoW artery diameter. We found that there was no significant different among CaDI, BCA and PCS (Figure 3A-3D). Then, we measure red blood cell (RBC) velocity by axial line scanning microscopy to analyze Tg(*kdrl:gfp;gata1:DsRed*)$^{zn1/sd2}$ zebrafish at 54 hpf, 3 and 4 dpf. The RBC velocity across CoW arteries was differentially distributed, with CaDI having the highest RBC velocity from 54 hpf to 4 dpf (Figure 3E-3G). This is consistent with CaDI being the inlet vessel for arterial blood flow within the entire CoW circulation. Next, we used computational fluid dynamics (CFD) to simulate the effect of flow on CoW, based on the Dextran-filled CoW geometric network and RBC velocity (ANSYS, 2014; Z. Chen et al., 2019; Fernandes et al., 2022). We found an overall increase in average WSS from 54 hpf to 4 dpf (Figure 3A-3C, and 3H). Further, the simulated flow pattern and WSS on the CoW showed that WSS in CaDI was significantly higher than BCA and PCS at 54 hpf, 3 dpf, and 4 dpf (Figure 3A-3C, 3I-3K). Moreover, upon comparing WSS with the number of acta2+ VSMCs per CoW arteries during the development, we observed a Pearson correlation coefficient of $r = 0.595$, indicating a moderate to strong positive correlation between these two variables (Figure S1C). In summary, the analysis of blood flow

suggests that CoW arteries undergo varied hemodynamic WSS, which correlates with the spatial and temporal pattern of VSMC differentiation along CoW arteries.

Blood flow is required for CoW artery muscularization

Our data suggest that ECs under arterial flow might favor *acta2*+ VSMC differentiation from *pdgfrb*+ progenitors. To test this hypothesis, we set up an *in vitro* cell co-culture experiment where GFP-PDGFRB+ human brain pericytes (GFP-HBVPs) were cultured in flow amenable outlet slides, then covered by a thin layer of collagen type 1. Confluent human endothelial cells (HUVECs) were seeded on top of that and then exposed to steady-state laminar or pulsatile flow conditions (Figure 4A) (Abello, Raghavan, Yien, & Stratman, 2022). Differentiation of PDGFRB+ human brain pericytes into ACTA2+ VSMCs was then quantified after 24 hours of flow treatment. We found that brain pericytes under pulsatile flow were larger and showed higher expression of VSMC differentiation markers including PDGFRB, ACTA2, and TRANSGELIN (Robin et al., 2013) (Figure 4B-4D), suggesting that pulsatile flow favored PDGFRB+ progenitor differentiation into VSMC.

Previous research suggests that blood flow is dispensable for recruitment of *pdgfrb*+ progenitors on BCA and PCS (Ando et al., 2016). To corroborate this, we injected 0.35 ng of *tnnt2a* morpholino antisense oligonucleotide (MO) into Tg(*pdgfrb:egfp*, *kdrl:hras-mcherry*)$^{ncv22/s896}$ at one to two-cell stage, to abrogate cardiac contractility and thus blood flow (Ando et al., 2016; Chi et al., 2008; Sehnert et al., 2002). Indeed, the number of *pdgfrb*+ cells on CaDI, BCA, and PCS at 3 dpf in *tnnt2a* morphants was comparable to uninjected sibling control, suggesting blood flow did not affect *pdgfrb*+ progenitor recruitment to CoW arteries (Figure S2G-S2H). To determine the effect of blood flow on VSMC differentiation, we injected *tnnt2a* MO into Tg(*acta2:mcherry*, *kdrl:gfp*)$^{ca8/zn1}$ (Cross, Cook, Lin, Chen, & Rubinstein, 2003; Sehnert et al., 2002; Whitesell et al., 2014). Notably, we found no *acta2*+ VSMCs on CoW arteries of *tnnt2a* morphants at either 3 or 4 dpf (Figure 4E-4F and 4H-4I), suggesting that blood flow was required for *acta2*+ VSMC differentiation on CoW arteries.

To further explore the temporal requirement of blood flow, we treated embryos with 25 μM nifedipine, a drug shown to reduce heart rate in zebrafish embryos (Figure S2A-S2C) (Gierten et al., 2020), from 54 hpf, right before the onset of *pdgfrb*+ progenitors' expression of *acta2* (Figure 2A-2C). We found that at 3 dpf the number of *acta2*+ VSMCs on the CaDI of treated embryos is greatly reduced (Figure 4G and 4J); *acta2*+ VSMCs on BCA and PCS at 4 dpf are also reduced significantly (Figure 4G and 4K), suggesting that blood flow reduction after 54 hpf impaired VSMC differentiation on CoW arteries.

To determine whether blood flow is required for short-term VSMC maintenance after differentiation on CoW arteries, we treated embryos with nifedipine from 4 dpf, after VSMC differentiation on CoW arteries, and imaged at 5 dpf. The number of *acta2*+ VSMCs on the CaDI and PCS in treated embryos was comparable to untreated controls (Figure S2D-S2F), suggesting that blood flow was required for differentiation but not for short-term maintenance of CoW VSMCs.

Blood flow-regulated transcription factor klf2a modulates CoW artery muscularization

Our results suggest that CoW ECs might express a flow dependent transcriptional program that regulates spatiotemporal dynamics of VSMC differentiation on CoW arteries. Previous studies showed that expression pattern of transcription factor *Klf2* in arterial ECs closely follow the pattern of flow induced WSS (Lee et al., 2006; Parmar et al., 2006). Consistently, higher *Klf2* expression can be induced by unidirectional pulsatile flow (Dekker et al., 2002). Furthermore, *klf2* is implicated in VSMC migration on arterial blood vessels during mouse development: loss of *klf2* leads to aorta VSMC deficiency (Wu, Bohanan, Neumann, & Lingrel, 2008). Interestingly, *klf2a* expression in primitive veins of zebrafish trunk prevents VSMC association (Stratman et al., 2020). Hence, we tested the hypothesis that *klf2a* might be spatiotemporally regulated in CoW ECs and modulate VSMC differentiation. We first imaged Tg(*klf2a:h2b-egfp*, *kdrl:hras-mcherry*)$^{ig11/s896}$, which labels nuclei with active *klf2a* signaling, and quantified the number of *klf2a*+ ECs in CoW arteries (Chi et al., 2008; Steed et al., 2016). To account for overall changes in EC number during

development (Ulrich, Ma, Baker, & Torres-Vazquez, 2011), and length of each vessel, we also imaged Tg(*fli1:nls-gfp*, *kdrl:hras-mcherry*)$^{y7/s896}$, which labels all EC nuclei (Figure S3A-S3I) (Roman et al., 2002). From 32 hpf to 54 hpf, the number of *klf2a*+ EC in CaDI was comparable to PCS (Figure 5A-5C), however, the number of *klf2a*+ ECs in CaDI was significantly higher than BCA and PCS from 3 dpf (Figure 5A and 5D-5E), when *acta2*+ VSMCs differentiated on CaDI but not BCA and PCS (Figure 2B-2C, 2F, and S1A-S1C). Pearson correlation comparing the number of *klf2a*+ ECs with the number of acta2+ VSMCs in CaDI, BCA and PCS at 3 dpf showed strong positive correlation with r = 0.974 (Figure S5J). These results suggest that the number of *klf2a*+ ECs in CoW arteries is spatially correlated with VSMC differentiation.

To further define the role of *klf2a* in VSMC differentiation on CoW arteries, we knocked down *klf2a* in Tg(*acta2:mcherry*, *kdrl:gfp*)$^{ca8/zn1}$ with 11 ng MO injection at one to two-cell stage and imaged at 3 to 4 dpf (Nicoli et al., 2010; Whitesell et al., 2014; Zhong et al., 2006). We validated the effect of *klf2a* MO knockdown with Tg(*klf2a:h2b-egfp*, *kdrl:hras-mcherry*)$^{ig11/s896}$ (Figure S3G-S3I) (Chi et al., 2008; Steed et al., 2016). Compared to uninjected control, *klf2a* morphants have significantly less *acta2*+ VSMCs on CaDI at 3 dpf but a normal number by 4 dpf (Figure 6A-6D), suggesting that *klf2a* knockdown delayed VSMC differentiation on CaDI. Together these data suggest that endothelial *klf2a* is required for the onset of VSMC differentiation on CoW arteries.

Discussion

In this study, we employed confocal live imaging of fluorescence transgenic zebrafish embryos to investigate the spatiotemporal dynamics of vascular smooth muscle cell (VSMC) differentiation on the cerebral vasculature (CoW), which comprises major arteries supplying blood to the vertebrate brain. Our observations revealed that CoW morphogenesis precedes the expression of arterial endothelial genes. Specifically, mural cell progenitors marked by pdgfrb+ initiate the expression of the VSMC marker acta2 subsequent to their recruitment to CoW arteries. Notably, VSMC differentiation occurs earlier in the anterior CoW arteries compared to their posterior counterparts, owing to the elevated wall shear stress (WSS) resulting from a higher velocity of red

blood cells in the incoming blood flow. To investigate the regulatory role of blood flow on the spatiotemporal dynamics of VSMC differentiation, we employed an in vitro co-culture assay along with genetic manipulation and drug treatments. Our findings indicate that blood flow indeed governs the timing and location of VSMC differentiation on CoW arteries. Moreover, we observed that the flow-responsive transcription factor klf2a is activated in a gradient manner from anterior to posterior CoW arteries, preceding the onset of VSMC differentiation. Knockdown experiments targeting klf2a revealed a delay in VSMC differentiation specifically in the anterior CoW arteries. Taken together, these findings highlight the role of endothelial klf2a activation by blood flow as a mechanism that promotes VSMC differentiation on CoW arteries within the brain (see Figure 7 for a visual summary).

Previous research shows that in zebrafish trunk, as soon as recruited to the dorsal aorta, VSMCs express *acta2* and *transgelin (tagln)*, suggesting simultaneous recruitment and differentiation from sclerotome progenitors (Ando et al., 2016; Stratman et al., 2017). On CoW arteries in zebrafish brain, however, VSMC differentiation occurs after *pdgfrb*+ progenitor recruitment and proceeds from anterior to posterior (Figure 2B-2F). The observed spatiotemporal dynamics of CoW VSMC differentiation again highlights organotypic development of blood vessels.

Our data suggests *klf2a* mediate blood flow regulation of VSMC differentiation on brain arteries, and thus raises the question of how *klf2a* transduces endothelial signals to mural cell progenitors and VSMCs. Notch signaling appears a plausible downstream effector of *klf2a* activation, as previous research suggests Notch responds to flow in heart valve development (Fontana et al., 2020), possibly downstream of *klf2* (Duchemin, Vignes, & Vermot, 2019). Wnt signaling is another possible downstream effector of *klf2a*, as previous research suggests endocardial *klf2* upregulates Wnt signaling in neighboring mesenchymal cells in heart valve development (Goddard et al., 2017). The roles of Notch and Wnt signaling in organotypic VSMC differentiation on brain arteries remain to be determined.

The expression of *klf2a* in CoW arterial ECs remained stable from 3 dpf to 4 dpf (Figure 5), which raises and interesting question on whether sustained *klf2a* expression

supports further maturation of VSMCs, as *acta2*+ VSMCs on CaDI showed distinct morphology at 4 dpf compared with 3 dpf, when they started differentiation from *pdgfrb*+ mural cell progenitors (Figure 2C-2D and S1). Previous research found that *acta2*+ VSMCs on the BCA and PCS express pericyte enriched *abcc9* (ATP binding cassette subfamily C member 9) at 4 dpf (Ando et al., 2022), when they started differentiation from *pdgfrb*+ mural cell progenitors and expressing *acta2*; *abcc9* expression is gradually lost from 5 dpf to 6 dpf (Ando et al., 2022). In addition, *acta2*+ VSMCs on CaDI, BCA, and PCS still retain expression of *pdgfrb* at 6 dpf (Ando et al., 2021). Thus, it is possible that stable expression of *klf2a* in CoW arterial ECs supports further VSMC maturation, as indicated by expression of *tagln* (Colijn, Nambara, & Stratman, 2023). Another aspect of VSMC maturation is its function to confer vascular tone. A previous study found that VSMC covered vessels in zebrafish brain dilate as early as 4 dpf and constrict at 6 dpf (Bahrami & Childs, 2020). Future study may focus on the association between expression of different VSMC markers and VSMC functional maturation.

Another question is how flow activates *klf2a* in brain arteries. In a hypoxia-induced pulmonary hypertension model, *klf2* is activated by G-protein coupled receptor mediated Apelin signaling (Chandra et al., 2011). In heart valve development, endocardial *klf2a* is upregulated by membrane bound mechanosensitive channels *trpp2* and *trpv4* (Heckel et al., 2015). The pathway through which flow activates *klf2a* in brain arterial ECs remains unknown. The CoW VSMC phenotype of *klf2a* morphants is similar to, but do not fully recapitulate the phenotypes of *tnnt2a* morphants or nifedipine treated embryos (Figure 4E-4L and Figure 6). A proximal explanation is compensation by paralogous *klf2b* in zebrafish. Further characterization of CoW VSMC development in *klf2a* and *klf2b* genetic mutants (Rasouli et al., 2018; Steed et al., 2016) may help determine whether *klf2b* compensates *klf2a* in CoW VSMC differentiation.

In addition to WSS, transmural pressure and associated mechanical stretch is another mechanical input of vascular wall that may contribute to VSMC differentiation. VSMCs autonomously sense and adapt to mechanical stretch (Haga, Li, & Chien, 2007). Cyclic stretching activates arterial VSMC production of certain components of extracellular matrix (ECM) (Leung, Glagov, & Mathews, 1976). In turn, specific

interactions between ECM and integrins enable VSMCs to sense mechanical stretch (Goldschmidt, McLeod, & Taylor, 2001; Wilson, Sudhir, & Ives, 1995). Connection to ECM is essential for VSMC force generation (Milewicz et al., 2017). VSMCs express stretch activated *trpp2*, which enables myogenic response to autoregulate resting arterial diameter (Sharif-Naeini et al., 2009). Interestingly, ex vivo stretching promotes expression of contractile proteins, such as *acta2* and *tagln* in VSMCs on murine portal veins (Albinsson, Nordstrom, & Hellstrand, 2004; Turczynska, Hellstrand, Sward, & Albinsson, 2013). In addition, excessive mechanical stretch promotes VSMC dedifferentiation and inflammation (Cao et al., 2017; Wang et al., 2018). Further investigation is needed to determine the potential role of increasing transmural pressure and associated mechanical stretch during development in VSMC differentiation.

There are a few limitations to our current study. Genetic manipulation and drug treatment that reduce heart rate would also reduce nutrients carried by blood flow, and the effects of nutrient and flow reduction could not be uncoupled in live zebrafish embryos. In addition, these methods are only capable of qualitative reduction of flow but not specific dampening of pulsations. *In vitro* three-dimensional (3D) vascular culture models, which combine ECs and mural cells (Mirabella et al., 2017; Vila Cuenca et al., 2021), could be further optimized to simulate complex geometry of brain arteries. Combining these models with microfluidics, which allows precise calibration of nutrient composition in culture media, flow velocity and pulse, would enable more thorough analysis of endothelial mechanotransduction and its contribution to VSMC differentiation (Abello, Raghavan, Yien, & Stratman, 2022; Gray & Stroka, 2017; Griffith et al., 2020).

We used nifedipine to temporally reduce heart rate and blood flow. Nifedipine is a blocker of L-type voltage-dependent calcium channels (VDCC) (Quevedo et al., 1998). A previous study shows that ML218, a T-type VDCC-selective inhibitor, tends to increase VSMC differentiation (Ando et al., 2022). In addition to the difference in drug targets, we also noted that in the previous study, the increase in VSMC differentiation only occur on anterior metencephalic central arteries (AMCtAs) that are more than 40 μm away from the BCA; these AMCtAs are much smaller than CoW arteries and have different geometry (Ando et al., 2022). Although the most obvious effect of nifedipine in

zebrafish embryos is heart rate and blood flow reduction (Gierten et al., 2020), it is possible that nifedipine affect VSMC through VDCCs. Further investigation is needed to uncouple the roles of different VDCCs in VSMC differentiation and their association with hemodynamics.

We used Tg(*flt4:yfp*, *kdrl:ras-mcherry*)$^{hu4881/s896}$ to show CoW arterial specification from primitive venous ECs (Chi et al., 2008; Hogan et al., 2009). *kdrl* is not the best arterial marker as its expression is only enriched but not restricted to arteries. While the use of the two fluorescence transgenic lines helped us establish the temporal sequence of CoW morphogenesis, arterial specification and VSMC differentiation, analysis of additional arterial and venous markers is needed to fully characterize arterial specification during vertebrate brain vascular development.

In summary, our work identifies flow induced endothelial *klf2a* activation as a mechanism that regulates spatiotemporal dynamics of VSMC differentiation on CoW arteries in the vertebrate brain. Our data may help advance approaches to regenerate differentiated VSMCs in cerebrovascular diseases. It would be important to further investigate mechanisms upstream and downstream of *klf2a* activation in brain arterial ECs and additional mechanotransduction pathways that may contribute to VSMC differentiation on brain arteries.

Material and Methods

Zebrafish husbandry and transgenic lines

Zebrafish were raised and maintained at 28.5 °C using standard methods. Protocols are approved by the Yale Institutional Animal Care and Use Committee (2020-11473). TgBAC(*pdgfrb:egfp*)^{ncv22} was generated by Ando et al., has been reported that the *pdgfrb:egfp*+ cells express other pericyte enriched marker abcc9 (ATP binding cassette subfamily C member 9) (Ando et al., 2016; Ando et al., 2019). By this transgenic line, they also observed that *pdgfrb* mutant lack brain pericytes and exhibit loss of vascular smooth muscle coverage (Ando et al., 2021). Thus, we used TgBAC(*pdgfrb:egfp*)^{ncv22} to

study mural cell coverage of vascular endothelium in zebrafish CoW arteries. All transgenic lines in Table 1 were established previously.

Table 1. List of zebrafish fluorescent transgenic lines used in the study

Transgenic Line	ID	Lab of Origin	Reference
Tg(*flt4:yfp*)^{hu4881}	ZDB-ALT-100208-1	S. Schulte-Merker	Hogan et al., 2009
Tg(*kdrl:hras-mcherry*)^{s896} [Tg(*kdrl:ras-mcherry*)^{s896}]	ZDB-ALT-081212-4	D.Y.R. Stainier	Chi et al., 2008
Tg(*acta2:mcherry*)^{ca8}	ZDB-ALT-120508-2	S.J. Childs	Whitesell et al., 2014
TgBAC(*pdgfrb:egfp*)^{ncv22}	ZDB-ALT-160609-1	N. Mochizuki	Ando et al., 2016
Tg(*kdrl:cerulean*)^{sd24}	ZDB-ALT-131024-2	D. Traver	Page et al., 2013
Tg(*kdrl:grcfp*)^{zn1} [Tg(*kdrl:gfp*)^{zn1}]	ZDB-ALT-051114-10	Zygogen Research Department	Cross et al., 2003
Tg(*klf2a:h2b-egfp*)^{ig11}	ZDB-ALT-161017-10	J. Vermot	Steed et al., 2016
Tg(*fli1:negfp*)^{y7} [Tg(*fli1:nls-gfp*)^{y7}]	ZDB-ALT-060821-4	B.M. Weinstein	Roman et al., 2002
Tg(*gata1:dsRed*)^{sd2}	ZDB-ALT-051223-6	L.I. Zon	Traver et al., 2003

385 Confocal fluorescence microscopy

Zebrafish embryos were raised in 0.003% 1-phenyl-2-thiourea (PTU, phenylthiocarbamide, or n-phenylthiourea, Sigma P7629) from gastrulation stage to prevent pigmentation. Embryos imaged live by confocal fluorescence microscopy were anesthetized in 0.1% tricaine methanesulfonate (TMS, MS-222, or Syncaine, Western Chemical, NC0872873) and mounted in 1% low melt agarose within glass bottom microwell dishes. Fluorescence images were captured with an upright Zeiss LSM 980 confocal microscope using a 20X objective.

Image analysis

Confocal fluorescence images were analyzed with Imaris microscopy image analysis software (Bitplane, Oxford Instruments). Average fluorescence intensity of mcherry in Tg(*flt4:yfp, kdrl:hras-mcherry*)$^{hu4881/s896}$ was estimated by generating volume objects covering the artery of interest with Surface module. Vessel lengths of the arteries were manually traced with Filament module. Numbers of *pdgfrb*+ mural cell progenitors, *acta2*+ vascular smooth muscle cells, and *klf2a*+ and *fli1*+ endothelial nucleus were counted with Spots module.

Morpholino injections

Morpholino antisense oligonucleotides were synthesized by Gene Tools. Morpholinos in Table 2 were validated previously. Optimized dose injected into each embryo are listed. Uninjected siblings were used as controls.

Table 2. List of morpholino antisense oligonucleotides used in the study

Morpholino	Sequence	ID	Reference	Dose (ng/embryo)
MO1-tnnt2a	5' - CATGTTTGCTCTGATCTGACACGCA - 3'	ZDB-MRPHLNO-060317-4	Sehnert et al., 2002	0.35

MO1-klf2a	5' - GGACCTGTCCAGTTCATCCTTCCAC - 3'	ZDB-MRPHLNO-100610-8	Nicoli et al., 2010	11

Nifedipine treatment

Nifedipine was dissolved into 20 mM in dimethyl sulfoxide (DMSO). The stock solution was diluted into 25 µM in egg water with 0.003% PTU to treat zebrafish embryos from 54 hpf to 3 dpf or 4 dpf. The stock solution was diluted into 20 µM in egg water with 0.003% PTU to treat zebrafish embryos from 4 dpf to 5 dpf. The same volume of DMSO was added into egg water with 0.003% PTU for sibling control embryos.

Microangiography

Embryos were anesthetized in 0.1% tricaine methanesulfonate, placed on an agarose mold, and injected pericardially with 4 nL Tetramethylrhodamine Dextran (2,000,000 molecular weight, Thermo Fisher) at a concentration of 10 mg/mL. Subsequently, the vasculature of embryos was checked for Dextran fluorescence signal under a stereomicroscope (Olympus, MVX10). Embryos with Dextran fluorescence were mounted in 1% low melt agarose within glass bottom microwell dishes and imaged with confocal microscope.

Red blood cell velocity

Red blood cell (RBC) velocity was measured by used axial line scanning to analyze zebrafish in the Tg*(kdrl:gfp;gata1:DsRed)*$^{zn1/sd2}$ background, in which blood vessels and RBCs are labeled with green and red fluorescent protein, respectively (Cross et al., 2003; Traver et al., 2003). As described previously (Barak et al., 2021), this axial line scan was conducted in a Zeiss LSM980 confocal microscope. A line was drawn inside the lumen of CoW vessels and parallel to the longitudinal axis of the vessel. The average length of the line was 21.21 µm. The scan speed was chosen as maximum per second for 20,000 cycles (total scan duration was 5.86 s; line scan time is 292.80 µs). A

kymograph was exported in TIFF format after every measurement by ZEN 3.5 and analyzed RBC recognition and segmentation by using Fiji (ImageJ). Firstly, the RBC kymography image was processed using 'noise despeckle' and 'enhance contrast' steps. The brightness and contrast were appropriately adjusted if needed. Next, the RBCs were segmented, thresholding was adjusted, and the slope of the RBCs was calculated automatically using the 'Analyze particle' option. Finally, the velocity of each RBC was calculated using the following equation: velocity = (1/tan(a)) $*$ (length of the y axis of the kymograph/duration of the total scan). We averaged systolic peak velocities and end diastolic velocities to measure the mean RBC velocity in the CoW vessels.

Computational fluid dynamic (CFD) simulation

Computational fluid dynamic (CFD) simulation was performed according to the geometry model of the circle of Willis (CoW) at 54 hpf, 3 and 4 dpf as previously described with modification (ANSYS, 2014; Barak et al., 2021). First, three-dimensional (3D) geometry models of CoW arteries were reconstructed from confocal z-stack microangiography images of Dextran injected Tg(*kdrl:gfp*) embryos with the Filament module in Imaris (9.9.0, Bitplane, Oxford instruments). These CoW 3D geometry models were pre-processed in ANSYS SpaceClaim 2022 R1 software. For example, the computational mesh on the CoW vascular wall was created and the boundary conditions were set up for the simulation. Meshing orthogonal quality was calculated, and objects less than 0.01 were excluded. Inlets and outlets were determined in the 3D model for the flow simulation. Next, the pre-processed models were imported in ANSYS Fluent 2022 R1 software. The non-Newtonian behavior of blood flow was modeled using the Carreau model which was provided by ANSYS. Blood density was considered as 1,060 kg/m^3. The computational simulation used average RBC velocity among the CoW arteries at 54 hpf (532.72 μm/s), 3 dpf (602.34 μm/s) and 4 dpf (552.83 μm/s), respectively. After the CoW geometry and numerical solution of blood flow were ready, the flow simulation was implemented with 200 iterations to identify the magnitude and distribution of the WSS in the CoW.

Cell Culture

Pooled primary Human Umbilical Vein Endothelial Cells (HUVEC) (PCS-100-010™, ATCC) were seeded at an initial concertation of 5,000 cells per cm^2, in 1x M119 media (110343-023, Gibco) supplemented with 16% FBS (Gibco), 84 µg/mL of heparin sodium salt (H3393, Sigma-Aldrich), 25 µg/mL of endothelial cell growth supplement (02-102, EMD Millipore Corp.) and 1x Antibiotic-antimycotic solution (15240-062, Gibco). Cell cultures were maintained at 37°C, 5% CO_2 and 95% humidity, until the cell reached 80% confluence.

To facilitate cell visualization in cell co-cultures, Human Brain Vascular Pericytes (HBVP) (1200, ScienCell) were transfected using lentiviral particles (LVP310, GenTarget, Inc.) to induce GFP expression under EF1a promotor. Cells cultures were initiated by seeding 5,000 cells per cm^2 in 175 cm^2 plastic flasks pre-coated with gelatin and 1x DMEM (11995-065, Gibco) supplemented with 10% FBS (Gibco), and 1x Antibiotic-antimycotic solution under the same cell culture conditions described above. When cell cultures were at 80% confluence, 200 µL containing 2 x 10^6 GFP-lentiviral particles were added to each 175 flasks. After 72 hours, fresh cell culture media supplemented with 10µg/mL of Blasticidin (15205, Sigma-Aldrich) were added to each flask to select the positive transfected cells.

Flow assays and immunostaining

HBVP cells were harvested and seeded at a concentration of 1.3 x 10^5 cells in 0.4 optical plastic flow microslides (80176, Ibidi) precoated with 1 mg/mL gelatin and incubated for 24 hours under standard culture conditions. After the initial incubation, 100 µg/mL of collagen I (354249, Corning) diluted in DMEM cell culture media was added to the slides to create a thin layer on top of the HBVP cells. After 2 hours, the media was removed and 2.5 x 10^5 HUVECs were seeded on top of the collagen I layer and incubated for additional 24 hours. After cell co-cultures were established, the slides were exposed to laminar (15 dyn/cm^2) or pulsatile (12-15 dyn/cm^2) flow for 24 hours, implementing a peristaltic pump adapted to produce different types of flow (Abello, Raghavan, Yien, & Stratman, 2022). After 24 hours, cultures were rinsed with 1x PBS and fixed for 30 minutes in 4% paraformaldehyde at room temperature. Cell cultures were immunostained with α-Smooth muscle actin D4K9N XP® rabbit monoclonal

antibody (19245, Cell Signaling), followed by Alexa Fluor 633 goat anti-rabbit IgG (A21071, Invitrogen). Confocal images were obtained using a 40x objective with a W1 Spinning Disk confocal microscope, a Fusion camera, and the Nikon Eclipse Ti2-E base. Fiji image processing software was used for image analysis and fluorescence intensity quantification.

Statistics

All statistical analyses were performed with GraphPad Prism (version 10.0.3). Mann–Whitney test was used to compare two groups to test mean differences (protein level, morpholino and nifedipine treatment). Two-way ANOVA followed by Tukey's multiple comparisons was used to test mean differences compared more than two groups under different conditions (average fluorescence intensity, cell number, vascular diameter). Ordinary one-way ANOVA with Tukey's multiple comparisons was used to test mean differences among three groups (RBC velocity, WSS, and cell number). Pearson correlation analysis was used to compare the strength and direction of a linear relationship between two variables with a covariance (WSS vs acta2+ EC, acta2+ EC vs klf2+ EC).

Acknowledgements

We thank the labs of S. Schulte-Merker, D.Y.R. Stainier, S.J. Childs, N. Mochizuki, D. Traver, J. Vermot, B.M Weinstein, and L.I. Zon for sharing zebrafish transgenic lines. We thank N. Semanchik for all the assistance with zebrafish adult colonies and husbandry. Experiments in the manuscript were supported by R01NS109160 and R01DK118728 awarded to S.N. and AHA23POST1025829 post-doctoral fellowship awarded to I.F.X. The paper is based on a dissertation submitted by S.C. to fulfill in part the requirements for the degree of Doctor of Philosophy, Yale University. S.C. was supported by a Gruber Science Fellowship from Yale Graduate School of Arts and Sciences.

Author Contributions

S.C. and I.F.X contributed to the experiments, the data analysis, and composed the figures. R.W. performed dextran microangiography experiments. J.A. and A.N.S. performed the *in vitro* experiments. S.C., I.F.X and S.N. wrote the manuscript and prepared figures. J.A. and A.N.S. edited the paper.

Figures and Figure Legends

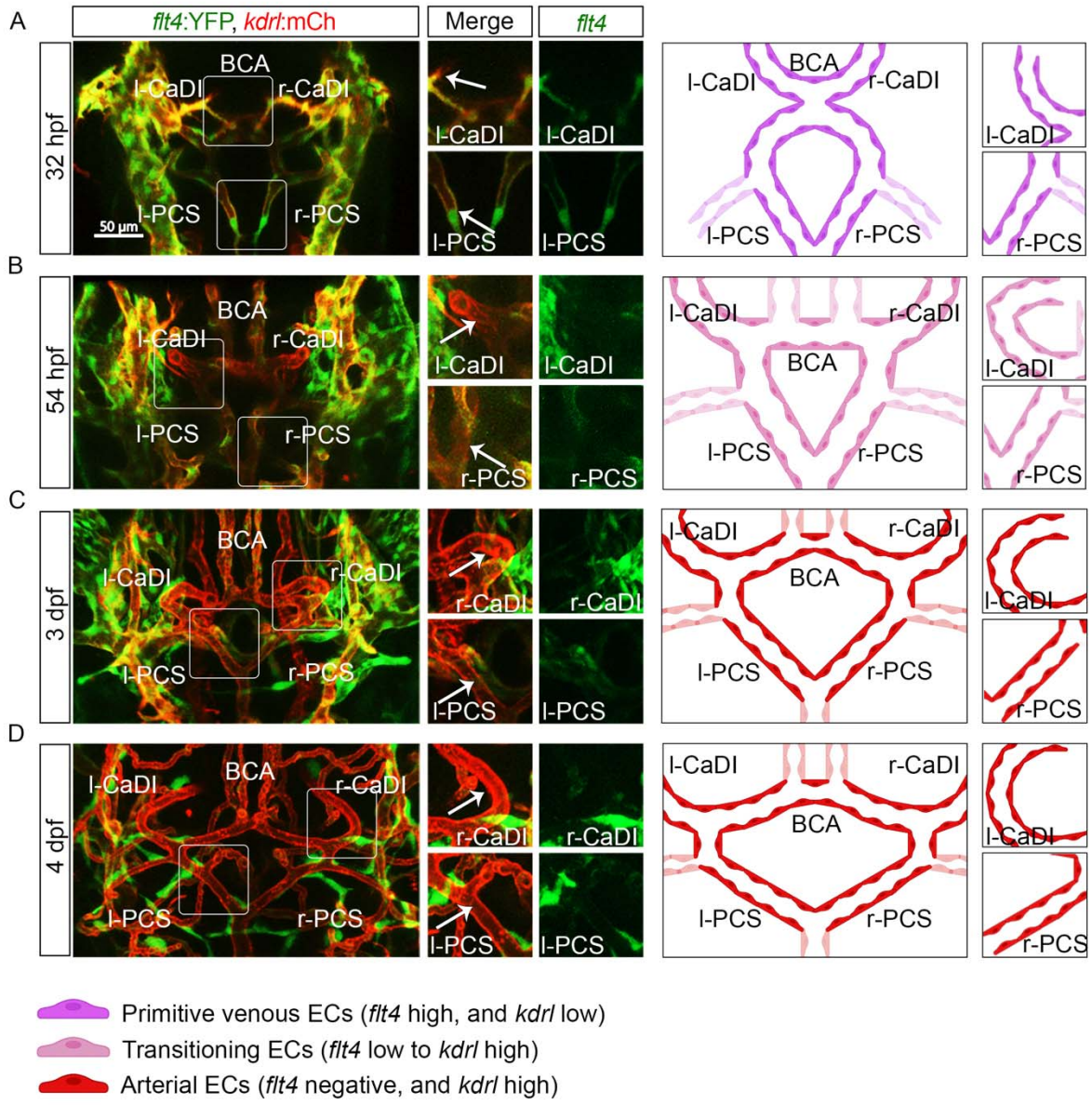
A
flt4:YFP, kdrl:mCh
Merge
flt4
32 hpf
BCA
l-CaDI
r-CaDI
l-PCS
r-PCS
50 µm
B
54 hpf
C
3 dpf
D
4 dpf
Primitive venous ECs (flt4 high, and kdrl low)
Transitioning ECs (flt4 low to kdrl high)
Arterial ECs (flt4 negative, and kdrl high)

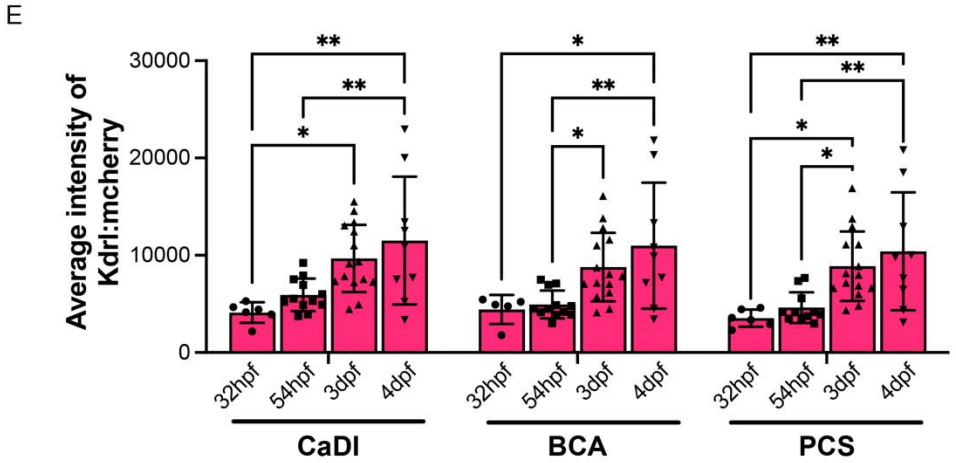
E
Average intensity of Kdrl:mcherry
30000
20000
10000
0
32hpf
54hpf
3dpf
4dpf
CaDI
BCA
PCS

Figure 1. Artery gene expression of endothelial cells (ECs) in circle of Willis (CoW) arteries

(A-D) Confocal live images of Tg(*flt4:yfp*, *kdrl:hras-mcherry*)$^{hu4881/s896}$ and scheme representation of CoW arteries in zebrafish brain at 32 hour post fertilization (hpf) (A), 54 hpf (B), 3 day post fertilization (dpf) (C), and 4 dpf (D). Green channel represents *flt4:yfp* fluorescence, Red channel represents *kdrl:hras-mcherry* fluorescence, and Merge panel combines both channels. Arrows point to the CoW arteries with *kdrl:hras-mcherry* signal. Scale bar = 50 µm

(E) Average intensity of *kdrl:hras-mcherry* in caudal division of internal carotid arteries (CaDI), basal communicating artery (BCA), and posterior communicating segments (PCS) at 32 hpf (n=6, 2 independent experiments), 54 hpf (n=12, 4 independent experiments), 3 dpf (n=15, 4 independent experiments), and 4 dpf (n=9, 2 independent experiments), two-way analyses of variance followed by Tukey's multiple comparisons, represented with mean ± SD, * $p \leq 0.05$, ** $p \leq 0.01$

Abbreviations: hpf: hour post fertilization, dpf: day post fertilization, EC: endothelial cell, l-CaDI: left caudal division of internal carotid artery, r-CaDI: right caudal division of internal carotid artery, BCA: basal communicating artery, l-PCS: left posterior communicating segment, r-PCS: right posterior communicating segment

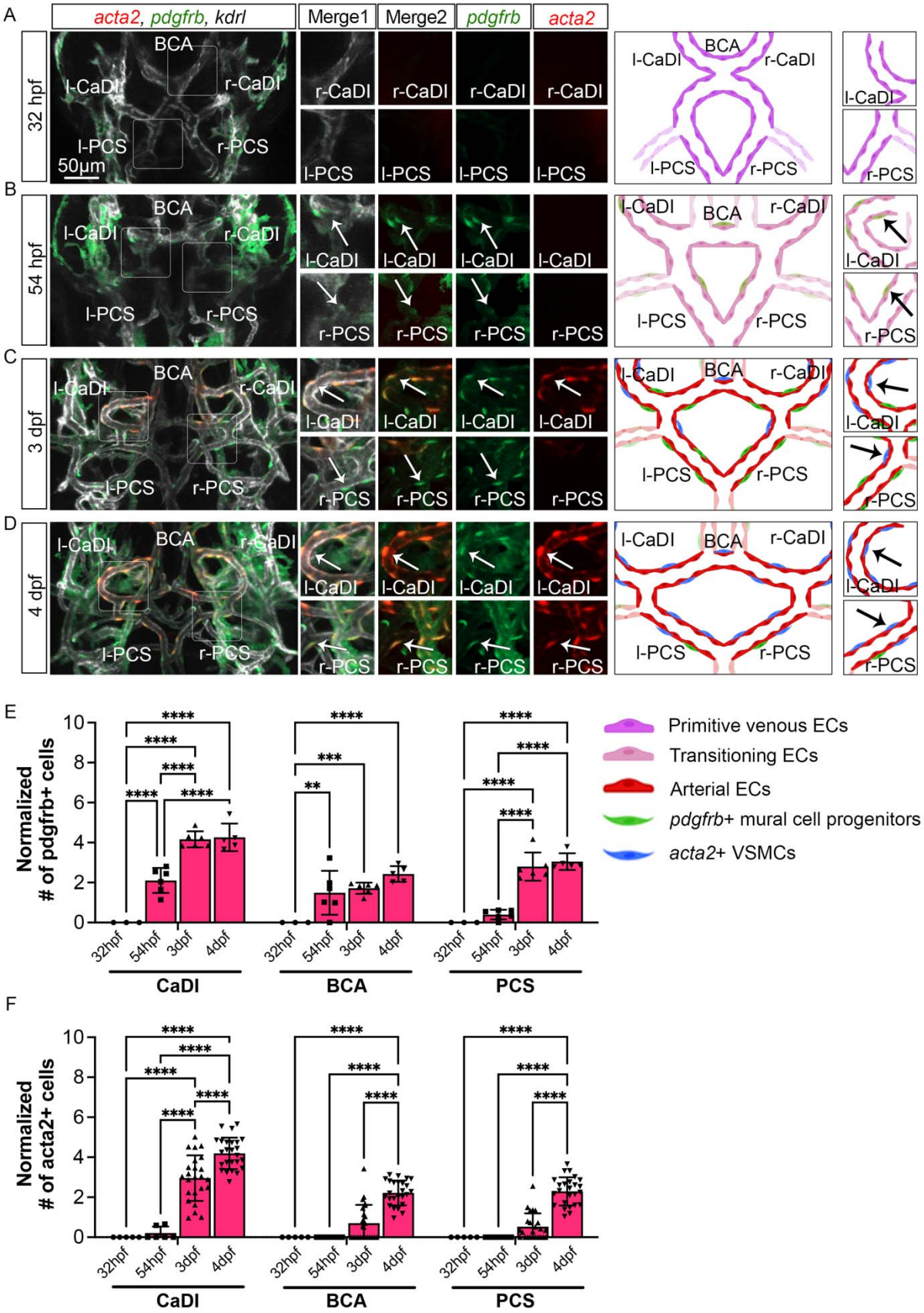
A
acta2, pdgfrb, kdrl
Merge1
Merge2
pdgfrb
acta2
32 hpf
BCA
l-CaDI
r-CaDI
l-PCS
r-PCS
50µm
B
54 hpf
C
3 dpf
D
4 dpf
E
Normalized # of pdgfrb+ cells
32hpf
54hpf
3dpf
4dpf
CaDI
BCA
PCS
Primitive venous ECs
Transitioning ECs
Arterial ECs
pdgfrb+ mural cell progenitors
acta2+ VSMCs
F
Normalized # of acta2+ cells

545

Figure 2. Vascular smooth muscle cell (VSMC) differentiation on circle of Willis (CoW) arteries

(A-D) Confocal live images of Tg(*acta2:mcherry*, *kdrl:cerulean*)$^{ca8/sd24}$ TgBAC(*pdgfrb:egfp*)^{ncv22} and scheme representation of vascular endothelium and mural cells on CoW arteries in zebrafish brain at 32 hour post fertilization (hpf) (A), 54 hpf (B), 3 day post fertilization (dpf) (C), and 4 dpf (D). White channel represents *kdrl:cerulean* fluorescence, Red channel represents *acta2:mcherry*, Green channel represents *pdgfrb:egfp,* Merge 1 panel combines all three channels, Merge 2 combines *acta2:mcherry* in red and *pdgfrb:egfp* in green. Arrows point to the CoW arteries with *pdgfrb:egfp* and *acta2:mcherry* signal. Scale bar = 50 µm

(E) Number of *pdgfrb*+ vascular mural cell progenitors per 100 µm vessel length on caudal division of internal carotid arteries (CaDI), basal communicating artery (BCA), and posterior communicating segments (PCS) at 32 hpf (n=3, 1 independent experiment), 54 hpf (n=6, 1 independent experiment), 3 dpf (n=6, 1 independent experiment), and 4 dpf (n=5, 1 independent experiment), two-way analyses of variance followed by Tukey's multiple comparisons, represented with mean ± SD, ** $p \leq 0.01$, *** $p \leq 0.001$, **** $p \leq 0.0001$

(F) Number of *acta2*+ VSMCs per 100 µm vessel length on CaDI, BCA, and PCS at 32 hpf (n=5, 1 independent experiment), 54 hpf (n=6, 2 independent experiments), 3 dpf (n=24, 6 independent experiments), and 4 dpf (n=25, 6 independent experiments), two-way analyses of variance followed by Tukey's multiple comparisons, represented with mean ± SD, **** $p \leq 0.0001$

Abbreviations: hpf: hour post fertilization, dpf: day post fertilization, EC: endothelial cell, VSMC: vascular smooth muscle cell, l-CaDI: left caudal division of internal carotid artery, r-CaDI: right caudal division of internal carotid artery, BCA: basal communicating artery, l-PCS: left posterior communicating segment, r-PCS: right posterior communicating segment

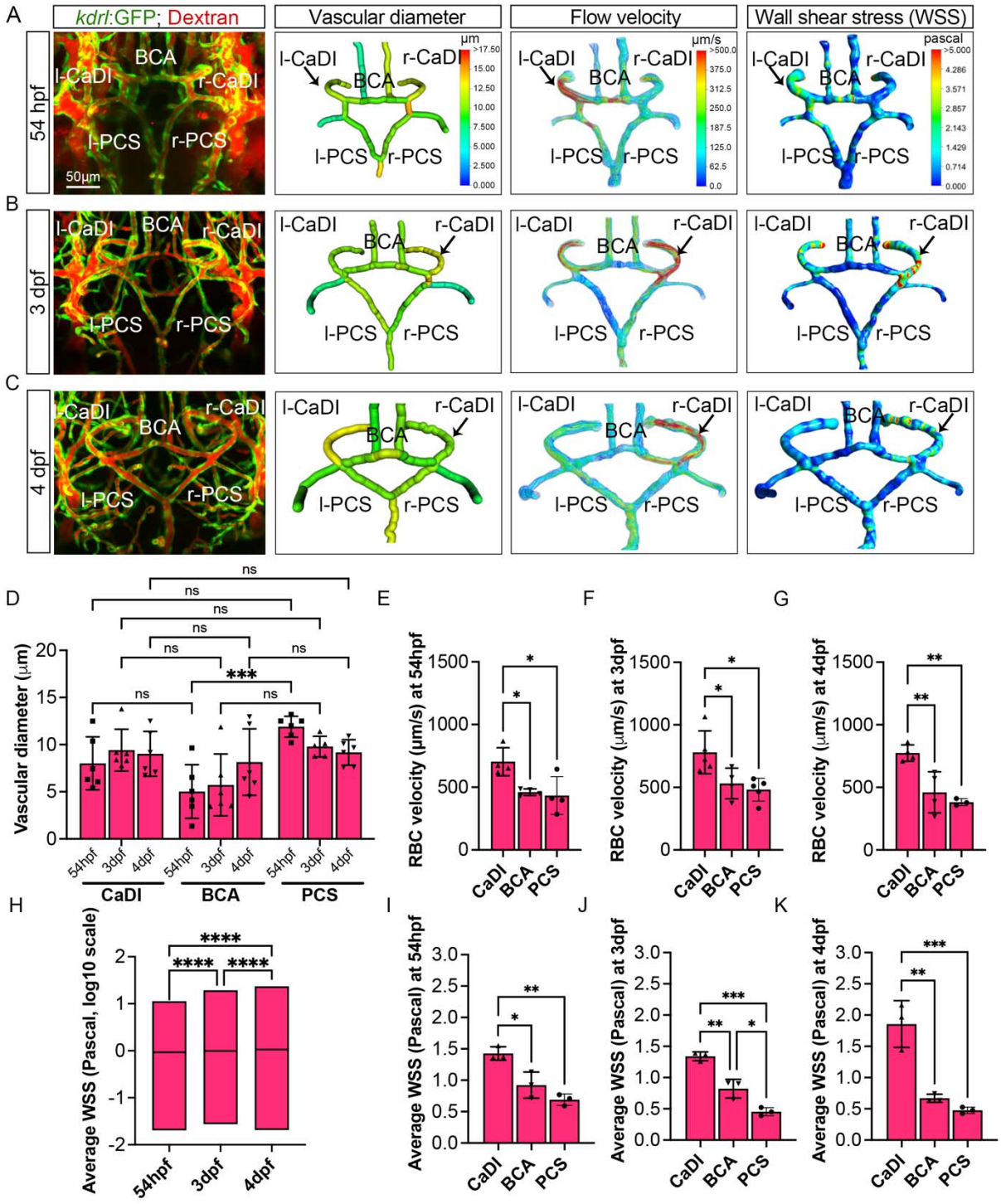
A
kdrl:GFP; Dextran
Vascular diameter
Flow velocity
Wall shear stress (WSS)
54 hpf
3 dpf
4 dpf
BCA
l-CaDI
r-CaDI
l-PCS
r-PCS
50µm
µm
µm/s
pascal
B
C
D
Vascular diameter (µm)
54hpf
3dpf
4dpf
CaDI
BCA
PCS
ns
***
E
F
G
RBC velocity (µm/s) at 54hpf
RBC velocity (µm/s) at 3dpf
RBC velocity (µm/s) at 4dpf
H
Average WSS (Pascal, log10 scale)
****
I
J
K
Average WSS (Pascal) at 54hpf
Average WSS (Pascal) at 3dpf
Average WSS (Pascal) at 4dpf

Figure 3. Computational fluid dynamic (CFD) simulation of circle of Willis (CoW) arteries

(A-C) Confocal live images of Tg(*kdrl:gfp*)^{zn1} injected with dextran and representation of vascular diameter, CFD simulated flow and wall shear stress (WSS) within the CoW arteries at 54 hour post fertilization (hpf) (A), 3 day post fertilization (dpf) (B), and 4 dpf (C). Arrows point to the CoW arteries with high flow velocity and WSS. Scale bar = 50 µm

(D) Average vascular diameter in caudal division of internal carotid arteries (CaDI), basal communicating artery (BCA), and posterior communicating segments (PCS) at 54 hpf (n=6, 1 independent experiment), 3 dpf (n=6, 1 independent experiment), and 4 dpf (n=6, 1 independent experiment), two-way analyses of variance followed by Tukey's multiple comparisons, *** p≤0.001

(E-G) Red blood cell (RBC) velocity in CaDI, BCA, and PCS at 54 hpf (n=4, 1 independent experiment) (E), 3 dpf (n=5, 1 independent experiment) (F), and 4 dpf (n=4, 1 independent experiment) (G), ordinary one-way ANOVA analyses with Tukey's multiple comparisons, represented with mean ± SD, * p≤0.05, ** p≤0.01

(H) Average wall shear stress (WSS) throughout the CoW arteries at 54 hpf (n=3, 1 independent experiment), 3 dpf (n=3, 1 independent experiment), and 4 dpf (n=3, 1 independent experiment), ordinary one-way ANOVA analyses with Tukey's multiple comparisons, **** p≤0.0001

(I-K) Average wall shear stress (WSS) in CaDI, BCA, and PCS at 54 hpf (n=3, 1 independent experiment) (I), 3 dpf (n=3, 1 independent experiment) (J), and 4 dpf (n=3, 1 independent experiment) (K), ordinary one-way ANOVA analyses with Tukey's multiple comparisons, represented with mean ± SD, * p≤0.05, ** p≤0.01, *** p≤0.001

Abbreviations: hpf: hour post fertilization, dpf: day post fertilization, RBC: red blood cell, WSS: wall shear stress, l-CaDI: left caudal division of internal carotid artery, r-CaDI: right caudal division of internal carotid artery, BCA: basal communicating artery, l-PCS: left posterior communicating segment, r-PCS: right posterior communicating segment

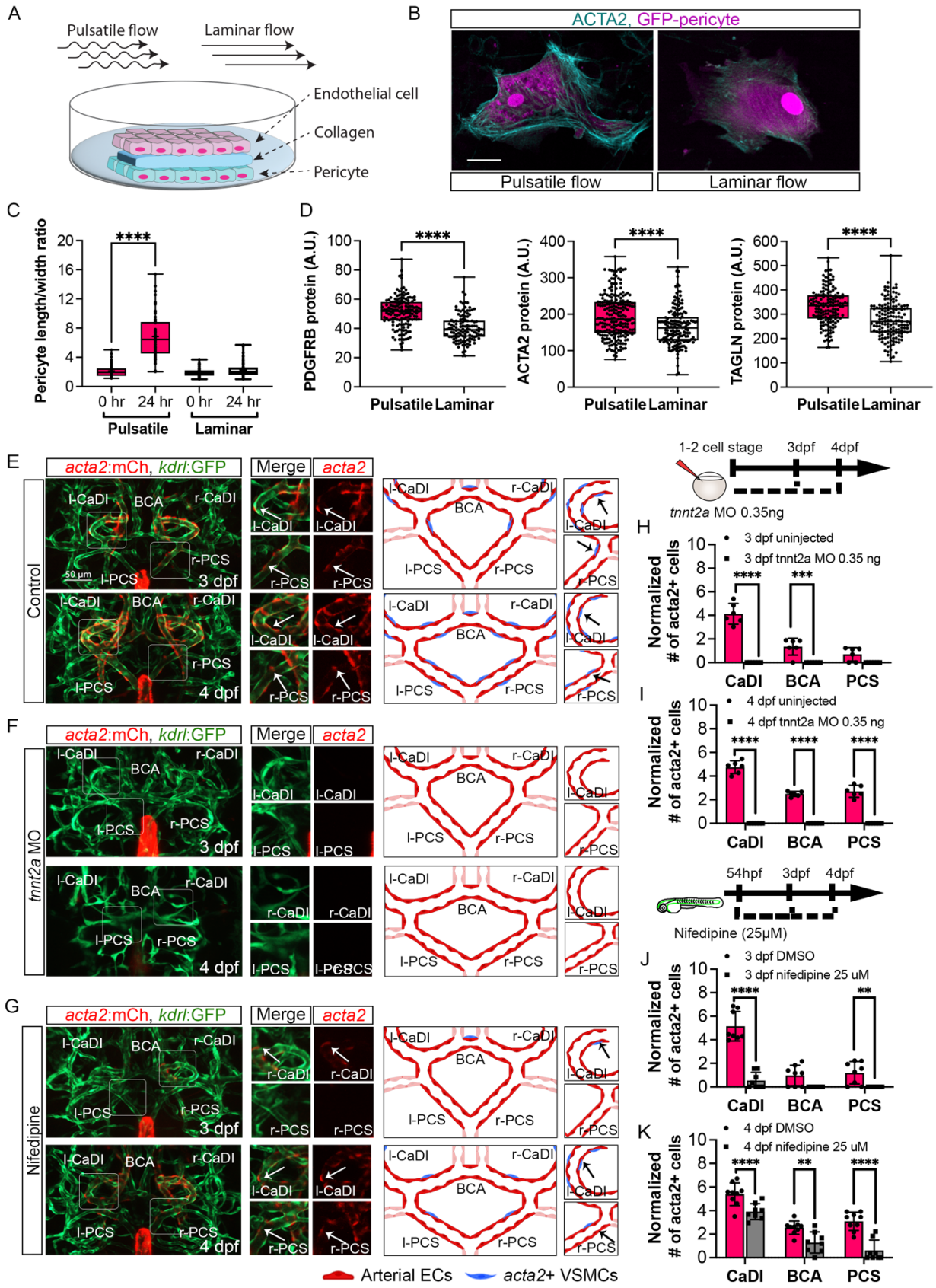
A
Pulsatile flow
Laminar flow
Endothelial cell
Collagen
Pericyte
B
ACTA2, GFP-pericyte
Pulsatile flow
Laminar flow
C
Pericyte length/width ratio
****
0 hr
24 hr
0 hr
24 hr
Pulsatile
Laminar
D
PDGFRB protein (A.U.)
ACTA2 protein (A.U.)
TAGLN protein (A.U.)
****
Pulsatile
Laminar
E
acta2:mCh, kdrl:GFP
Merge
acta2
Control
l-CaDI
BCA
r-CaDI
l-PCS
r-PCS
50 µm
3 dpf
4 dpf
F
tnnt2a MO
G
Nifedipine
Arterial ECs
acta2+ VSMCs
1-2 cell stage
3dpf
4dpf
tnnt2a MO 0.35ng
H
3 dpf uninjected
3 dpf tnnt2a MO 0.35 ng
Normalized # of acta2+ cells
CaDI
BCA
PCS
I
4 dpf uninjected
4 dpf tnnt2a MO 0.35 ng
54hpf
Nifedipine (25µM)
J
3 dpf DMSO
3 dpf nifedipine 25 uM
K
4 dpf DMSO
4 dpf nifedipine 25 uM

Figure 4. Blood flow is required for vascular smooth muscle cell (VSMC) differentiation on circle of Willis (CoW) arteries

(A) Scheme representation of *in vitro* cell co-culture experiment

(B) Representative immunofluorescence images of brain pericytes after exposure of pulsative flow and laminar flow. Cells were stained for ACTA2 (cyan), and cytosolic GFP label (magenta). Scale bar = 10 µm

(C) Morphological measurement of brain pericyte length/width ratio before and after exposure of pulsative flow and laminar flow (n = 63 cells), two-tailed Mann–Whitney test, represented with mean ± SD, **** p≤0.0001

(D) Protein level of PDGFRB (n = 153 cells), ACTA2 (n = 222 cells), and TAGLN (n = 150 cells) in arbitrary unit (A.U.) after exposure of pulsative flow and laminar flow, two-tailed Mann–Whitney test, represented with mean ± SD, **** p≤0.0001

(E-G) Confocal live images of Tg(*acta2:mcherry*; *kdrl:gfp*)$^{ca8/zn1}$ and scheme representation of vascular endothelium and VSMCs on CoW arteries at 3 day post fertilization (dpf) and 4 dpf in control embryos (E), embryos injected with 0.35 ng *tnnt2a* morpholino (MO) (F), and embryos treated with 25 µM nifedipine from 54 hpf (G). Red channel represents *acta2:mcherry*, Green channel represents *kdrl:gfp*, and Merge panel combines both channels. Arrows point to the CoW arteries with *acta2:mcherry* signal. Scale bar = 50 µm

(H) Number of *acta2*+ VSMCs per 100 µm vessel length on caudal division of internal carotid arteries (CaDI), basal communicating artery (BCA), and posterior communicating segments (PCS) at 3 dpf in uninjected control (n=6, 1 independent experiment) and embryos injected with 0.35 ng *tnnt2a* MO at one to two cell stage (n=6, 1 independent experiment), two-tailed Mann–Whitney test on each vessel's comparison, represented with mean ± SD, *** p≤0.001, **** p≤0.0001

(I) Number of *acta2*+ VSMCs per 100 µm vessel length on CaDI, BCA, and PCS at 4 dpf in uninjected control (n=6, 1 independent experiment) and embryos injected with 0.35 ng *tnnt2a* MO at one to two cell stage (n=6, 1 independent experiment), two-tailed

Mann–Whitney test on each vessel's comparison, represented with mean ± SD, **** p≤0.0001

(I) Number of *acta2*+ VSMCs per 100 μm vessel length on CaDI, BCA, and PCS at 3 dpf in DMSO control (n=8, 2 independent experiments) and embryos treated with 25 μM nifedipine from 54 hpf (n=8, 2 independent experiments), two-tailed Mann–Whitney test on each vessel's comparison, represented with mean ± SD, ** p≤0.01, **** p≤0.0001

(J) Number of *acta2*+ VSMCs per 100 μm vessel length on CaDI, BCA, and PCS at 4 dpf in DMSO control (n=9, 2 independent experiments) and embryos treated with 25 μM nifedipine from 54 hpf (n=8, 2 independent experiments), two-tailed Mann–Whitney test on each vessel's comparison, represented with mean ± SD, ** p≤0.01, **** p≤0.0001

Abbreviations: hpf: hour post fertilization, dpf: day post fertilization, EC: endothelial cell, VSMC: vascular smooth muscle cell, MO: morpholino, l-CaDI: left caudal division of internal carotid artery, r-CaDI: right caudal division of internal carotid artery, BCA: basal communicating artery, l-PCS: left posterior communicating segment, r-PCS: right posterior communicating segment

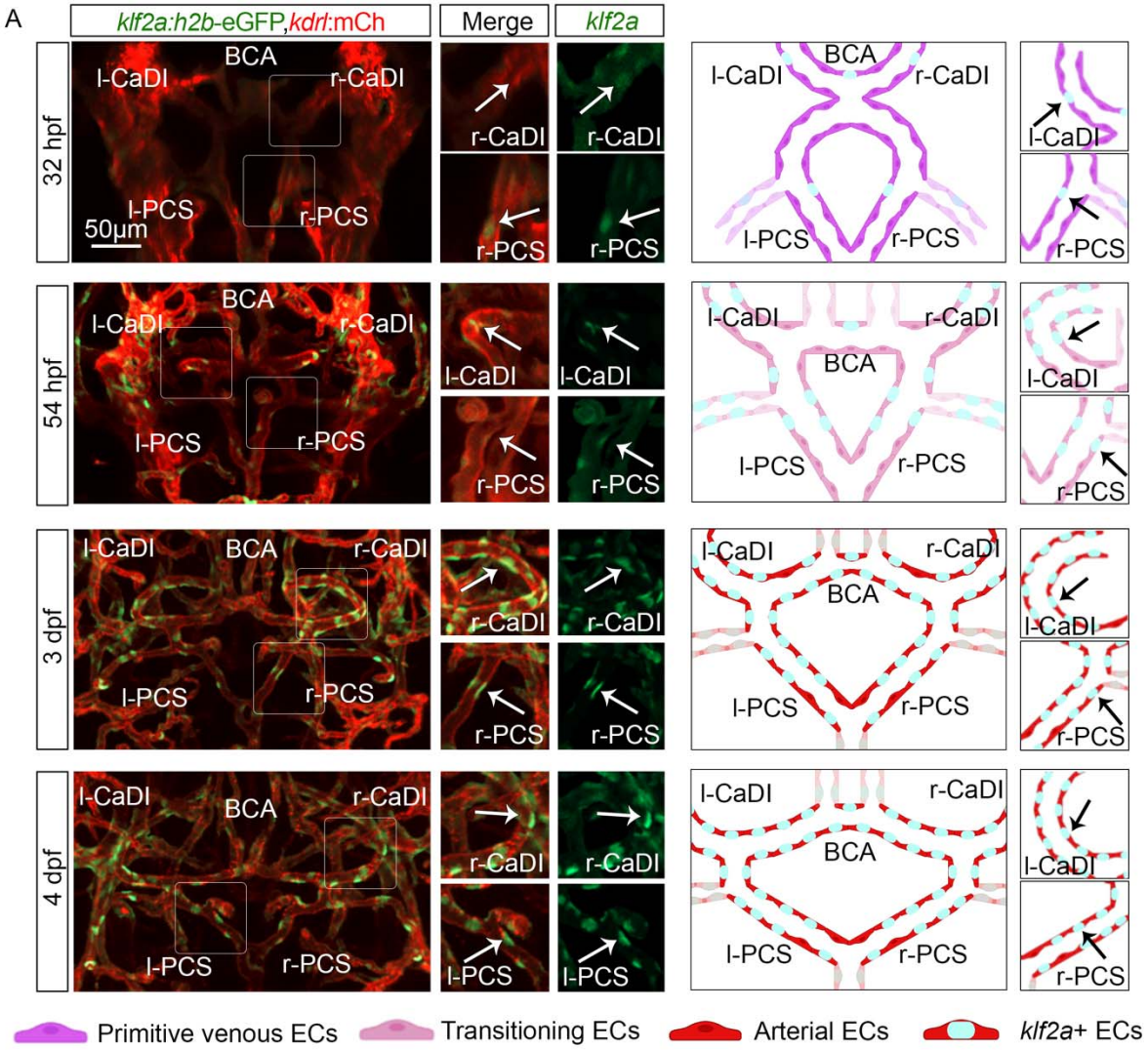
A
klf2a:h2b-eGFP,kdrl:mCh
Merge
klf2a
32 hpf
54 hpf
3 dpf
4 dpf
BCA
l-CaDI
r-CaDI
l-PCS
r-PCS
50µm
Primitive venous ECs
Transitioning ECs
Arterial ECs
klf2a+ ECs

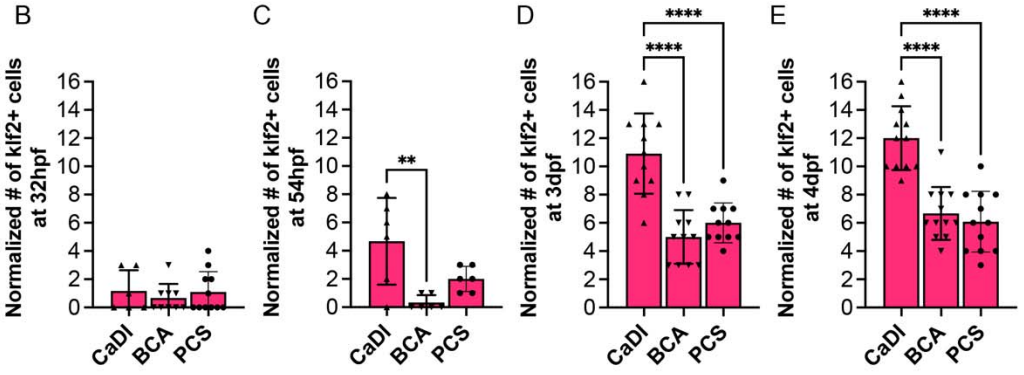
B
C
D
E
Normalized # of klf2+ cells at 32hpf
Normalized # of klf2+ cells at 54hpf
Normalized # of klf2+ cells at 3dpf
Normalized # of klf2+ cells at 4dpf
CaDI
BCA
PCS
**
****

Figure 5. Blood flow regulated transcription factor *klf2a* is expressed in circle of Willis (CoW) arteries

(A) Confocal live images of Tg(*klf2a:h2b-gfp*, *kdrl:ras-mcherry*)$^{ig11/s896}$ and scheme representation of endothelial cells (ECs) in CoW arteries in zebrafish brain at 32 hour post fertilization (hpf), 54 hpf, 3 day post fertilization (dpf), and 4 dpf. Green channel represents *klf2a:h2b-gfp*, Red channel represents *kdrl:ras-mcherry*, and Merge panel combines both channels. Arrows point to the CoW arteries with *klf2a:h2b-gfp* signal. Scale bar = 50 µm

(B-E) Number of *klf2a*+ ECs per 100 µm vessel length on caudal division of internal carotid arteries (CaDI), basal communicating artery (BCA), and posterior communicating segments (PCS) at 32 hpf (n=6, 3 independent experiments) (B), 54 hpf (n=6, 2 independent experiments) (C), 3 dpf (n=11, 3 independent experiments) (D), and 4 dpf (n=12, 3 independent experiments) (E), ordinary one-way ANOVA analyses with Tukey's multiple comparisons, represented with mean ± SD, ** $p \leq 0.01$, **** $p \leq 0.0001$

Abbreviations: hpf: hour post fertilization, dpf: day post fertilization, EC: endothelial cell, l-CaDI: left caudal division of internal carotid artery, r-CaDI: right caudal division of internal carotid artery, BCA: basal communicating artery, l-PCS: left posterior communicating segment, r-PCS: right posterior communicating segment

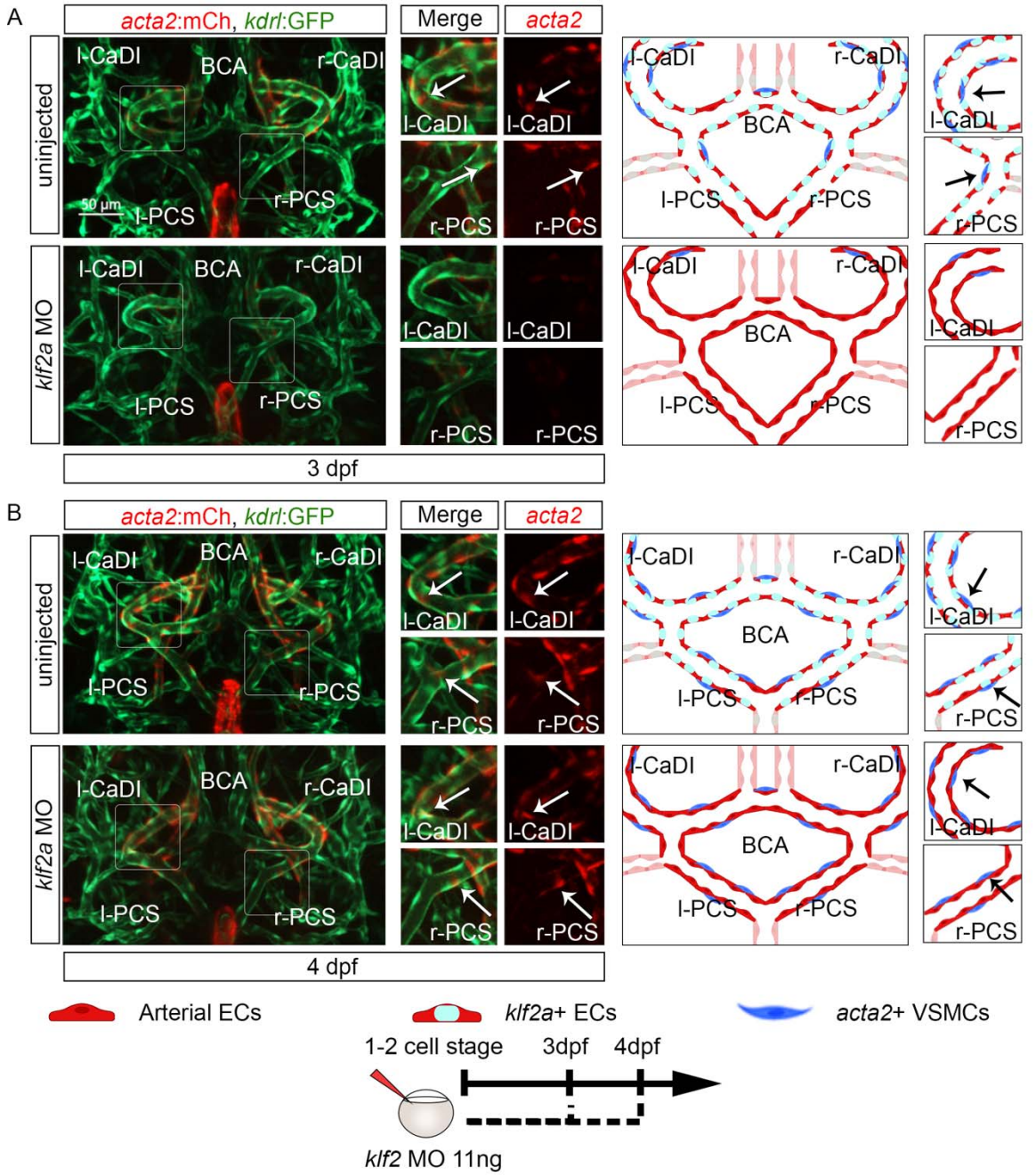
A
acta2:mCh, kdrl:GFP
Merge
acta2
uninjected
klf2a MO
l-CaDI
BCA
r-CaDI
l-PCS
r-PCS
50 µm
3 dpf
B
4 dpf
Arterial ECs
klf2a+ ECs
acta2+ VSMCs
1-2 cell stage
3dpf
4dpf
klf2 MO 11ng

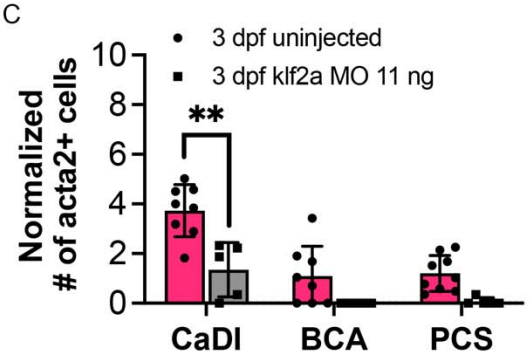
C
3 dpf uninjected
3 dpf klf2a MO 11 ng
Normalized # of acta2+ cells
**
CaDI
BCA
PCS

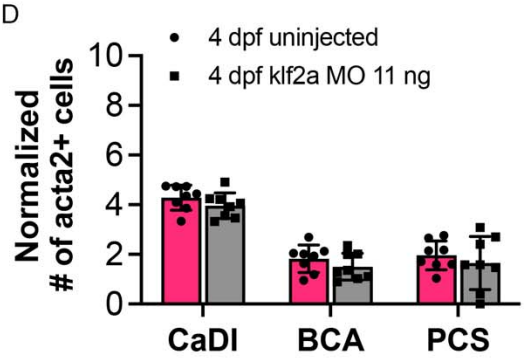
D
4 dpf uninjected
4 dpf klf2a MO 11 ng
Normalized # of acta2+ cells
CaDI
BCA
PCS

Figure 6. *klf2a* promotes vascular smooth muscle cell (VSMC) differentiation on anterior circle of Willis (CoW) arteries

(A-B) Confocal live images of Tg(*acta2:mcherry*; *kdrl:gfp*)$^{ca8/zn1}$ and scheme representation of vascular endothelium and VSMCs on CoW arteries at 3 day post fertilization (dpf) (A) and 4 dpf (B) in uninjected control embryos, embryos injected with 11 ng *klf2a* morpholino (MO). Red channel represents *acta2:mcherry*, Green channel represents *kdrl:gfp*, and Merge panel combines both channels. Arrows point to the CoW arteries with *acta2:mcherry* signal. Scale bar = 50 µm

(C) Number of *acta2*+ VSMCs per 100 µm vessel length on caudal division of internal carotid arteries (CaDI), basal communicating artery (BCA), and posterior communicating segments (PCS) at 3 dpf in uninjected control (n=8, 2 independent experiments) and embryos injected with 11 ng *klf2a* MO at one to two cell stage (n=8, 2 independent experiments), two-tailed Mann–Whitney test on each vessel's comparison, represented with mean ± SD, ** p≤0.01

(D) Number of *acta2*+ VSMCs per 100 µm vessel length on CaDI, BCA, and PCS at 4 dpf in uninjected control (n=8, 3 independent experiments) and embryos injected with 11 ng *klf2a* MO at one to two cell stage (n=8, 3 independent experiments), two-tailed Mann–Whitney test on each vessel's comparison, represented with mean ± SD

Abbreviations: hpf: hour post fertilization, dpf: day post fertilization, EC: endothelial cell, l-CaDI: left caudal division of internal carotid artery, r-CaDI: right caudal division of internal carotid artery, BCA: basal communicating artery, l-PCS: left posterior communicating segment, r-PCS: right posterior communicating segment

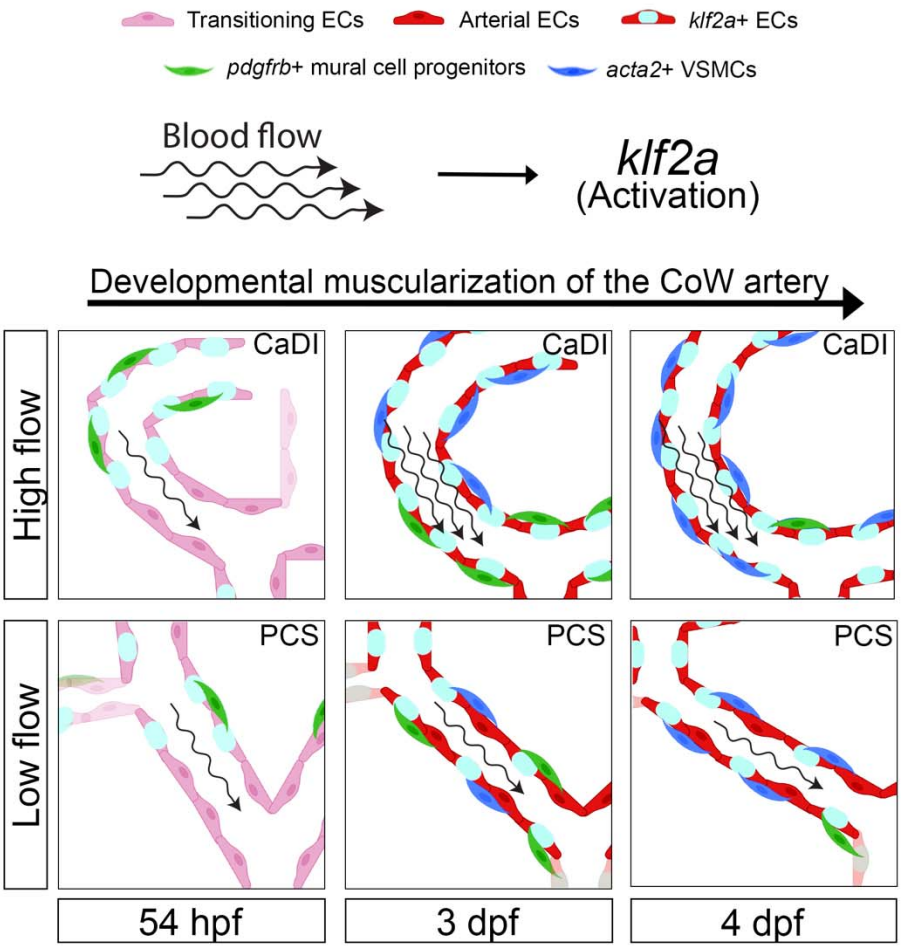
Transitioning ECs
Arterial ECs
klf2a+ ECs
pdgfrb+ mural cell progenitors
acta2+ VSMCs
Blood flow
klf2a
(Activation)
Developmental muscularization of the CoW artery
High flow
Low flow
CaDI
PCS
54 hpf
3 dpf
4 dpf

690

Figure 7. Schematic model of the developmental muscularization of the CoW arteries

The model shows how blood flow generate higher hemodynamics in anterior CoW arteries like the caudal division of internal carotid artery (CaDI) via the activation of endothelial *klf2a* signaling. Other posterior CoW arteries with straight shape like the posterior communicating segment (PCS) experience less hemodynamic force and showed moderate *klf2a* activation and VSMC differentiation.

Abbreviations: hpf: hour post fertilization, dpf: day post fertilization, EC: endothelial cell, VSMC: vascular smooth muscle cell, CaDI: caudal division of internal carotid artery, PCS: posterior communicating segment

Supplementary Figures and Supplementary Figure Legends

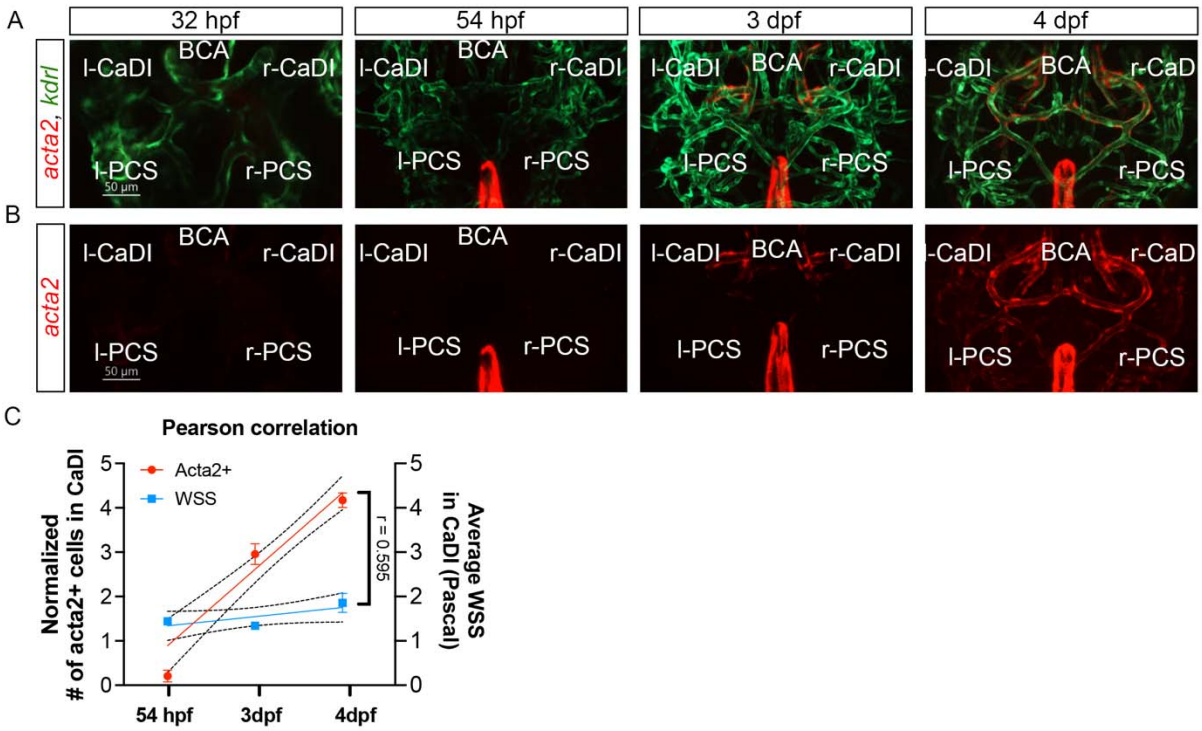
A
32 hpf
54 hpf
3 dpf
4 dpf
acta2, kdrl
BCA
l-CaDI
r-CaDI
l-PCS
r-PCS
50 µm
B
acta2
C
Pearson correlation
Acta2+
WSS
Normalized
# of acta2+ cells in CaDI
Average WSS
in CaDI (Pascal)
r = 0.595
54 hpf
3dpf
4dpf

Figure S1. Vascular smooth muscle cell (VSMC) differentiation on circle of Willis (CoW) arteries

(A-B) Confocal live images of Tg(*acta2:mcherry*, *kdrl:gfp*)$^{ca8/zn1}$ in CoW arteries of zebrafish brain at 32 hour post fertilization (hpf), 54 hpf, 3 day post fertilization (dpf), and 4 dpf. Red channel represents *acta2:mcherry*, Green channel represents *kdrl:gfp*, and Merge panel combines both channels. Scale bar = 50 μm

(C) Linear regression with normalized # acta2+ cells in CaDI (left y-axis) and average wall shear stress (WSS) (right y-axis) with the developmental stages (54 hpf, 3 and 4 dpf, x-axis), and Pearson correlation coefficient (r) is provided, indicating the degree of linear relationship between two variables.

Abbreviations: hpf: hour post fertilization, dpf: day post fertilization, VSMC: vascular smooth muscle cell, l-CaDI: left caudal division of internal carotid artery, r-CaDI: right caudal division of internal carotid artery, BCA: basal communicating artery, l-PCS: left posterior communicating segment, r-PCS: right posterior communicating segment

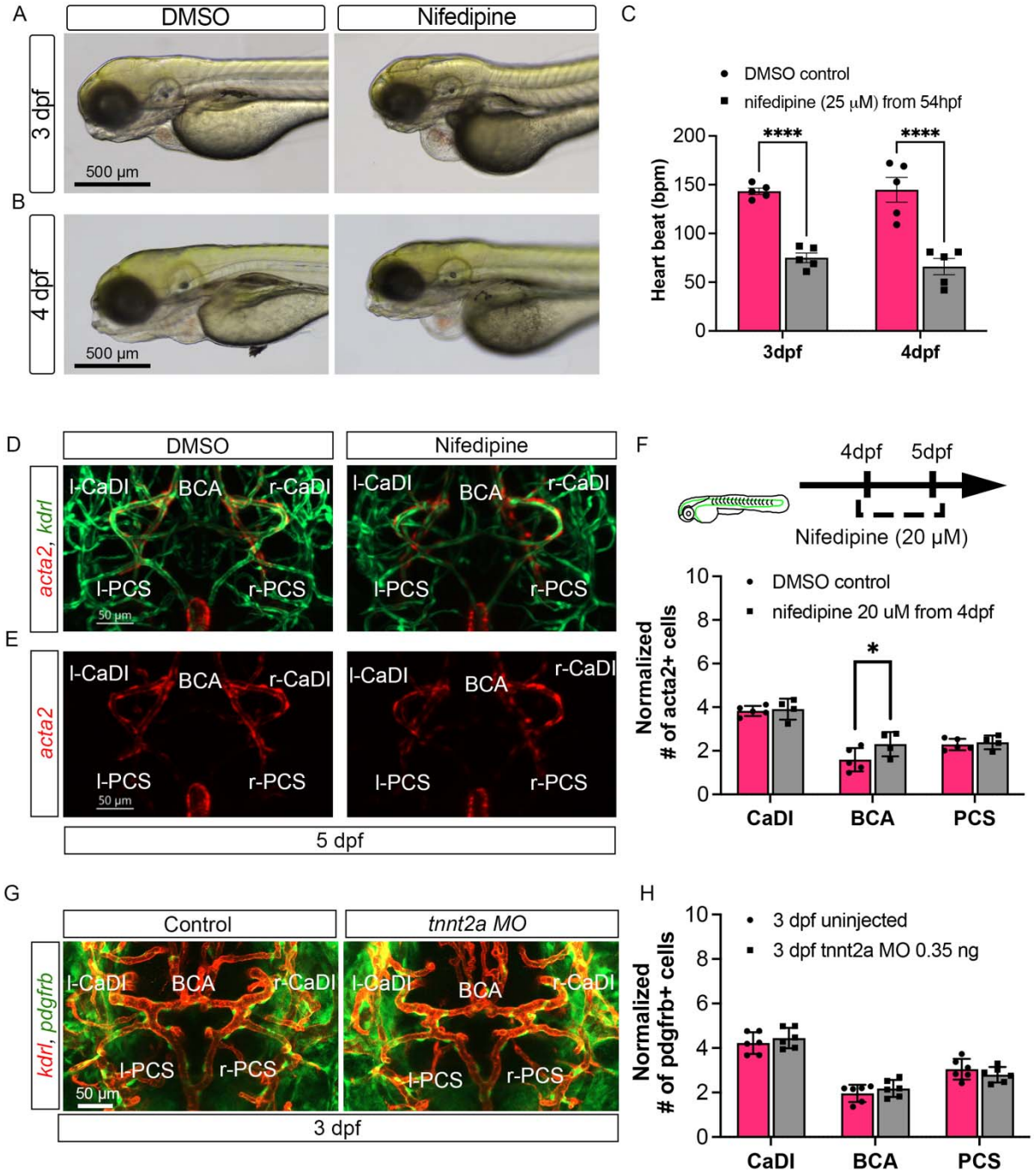
A
DMSO
Nifedipine
3 dpf
4 dpf
500 µm
B
C
DMSO control
nifedipine (25 µM) from 54hpf
Heart beat (bpm)
****
3dpf
4dpf
D
acta2, kdrl
l-CaDI
BCA
r-CaDI
l-PCS
r-PCS
50 µm
E
acta2
5 dpf
F
4dpf
5dpf
Nifedipine (20 µM)
DMSO control
nifedipine 20 uM from 4dpf
Normalized # of acta2+ cells
*
CaDI
BCA
PCS
G
Control
tnnt2a MO
kdrl, pdgfrb
3 dpf
H
3 dpf uninjected
3 dpf tnnt2a MO 0.35 ng
Normalized # of pdgfrb+ cells

Figure S2. Blood flow is not required for vascular smooth muscle cell (VSMC) maintenance or *pdgfrb*+ mural cell progenitor recruitment on circle of Willis (CoW) arteries

(A-B) Bright-field images of Tg(*acta2:mcherry*; *kdrl:gfp*)$^{ca8/zn1}$ in control embryos treated with DMSO and embryos treated with 25 µM nifedipine from 54 hour post fertilization (hpf) at 3 day post fertilization (dpf) (A) and 4 dpf (B). Scale bar = 500 µm

(C) Quantitative heartbeat rate at 3 dpf and 4 dpf in DMSO control embryos and embryos treated with 25 µM nifedipine from 54 hpf (n=5 each group, 1 independent experiment), two-tailed Mann–Whitney test on each vessel's comparison, represented with mean ± SD, **** p≤0.0001

(D-E) Confocal live images of Tg(*acta2:mcherry*; *kdrl:gfp*)$^{ca8/zn1}$ in CoW arteries of zebrafish brain at 5 dpf in DMSO control embryos and embryos treated with 20 µM nifedipine from 4 dpf. Red channel represents *acta2:mcherry*, Green channel represents *kdrl:gfp*, and Merge panel combines both channels. Scale bar = 50 µm

(F) Number of *acta2*+ VSMCs per 100 µm vessel length on caudal division of internal carotid arteries (CaDI), basal communicating artery (BCA), and posterior communicating segments (PCS) at 5 dpf in DMSO control (n=5, 1 independent experiment) and embryos treated with 20 µM nifedipine from 4 dpf (n=4, 1 independent experiment), two-tailed Mann–Whitney test on each vessel's comparison, represented with mean ± SD, * p≤0.05

(G) Confocal live images of Tg(*pdgfrb:egfp, kdrl:ras-mcherry*)$^{ncv22/s896}$ labeling vascular endothelium and *pdgfrb*+ vascular mural cell progenitors on the CoW arteries in zebrafish brain at 3 dpf. Red channel represents *kdrl:ras-mcherry*, Green channel represents *pdgfrb:egfp.* Scale bar = 50 µm

(H) Number of *pdgfrb*+ vascular mural cell progenitors per 100 µm vessel length on CaDI, BCA, and PCS in control embryos and embryos injected with 0.35 ng *tnnt2a* morpholino (MO) at 3 dpf (n=6, 1 independent experiment), two-way analyses of variance followed by Tukey's multiple comparisons, represented with mean ± SD.

Abbreviations: hpf: hour post fertilization, dpf: day post fertilization, VSMC: vascular smooth muscle cell, l-CaDI: left caudal division of internal carotid artery, r-CaDI: right caudal division of internal carotid artery, BCA: basal communicating artery, l-PCS: left posterior communicating segment, r-PCS: right posterior communicating segment

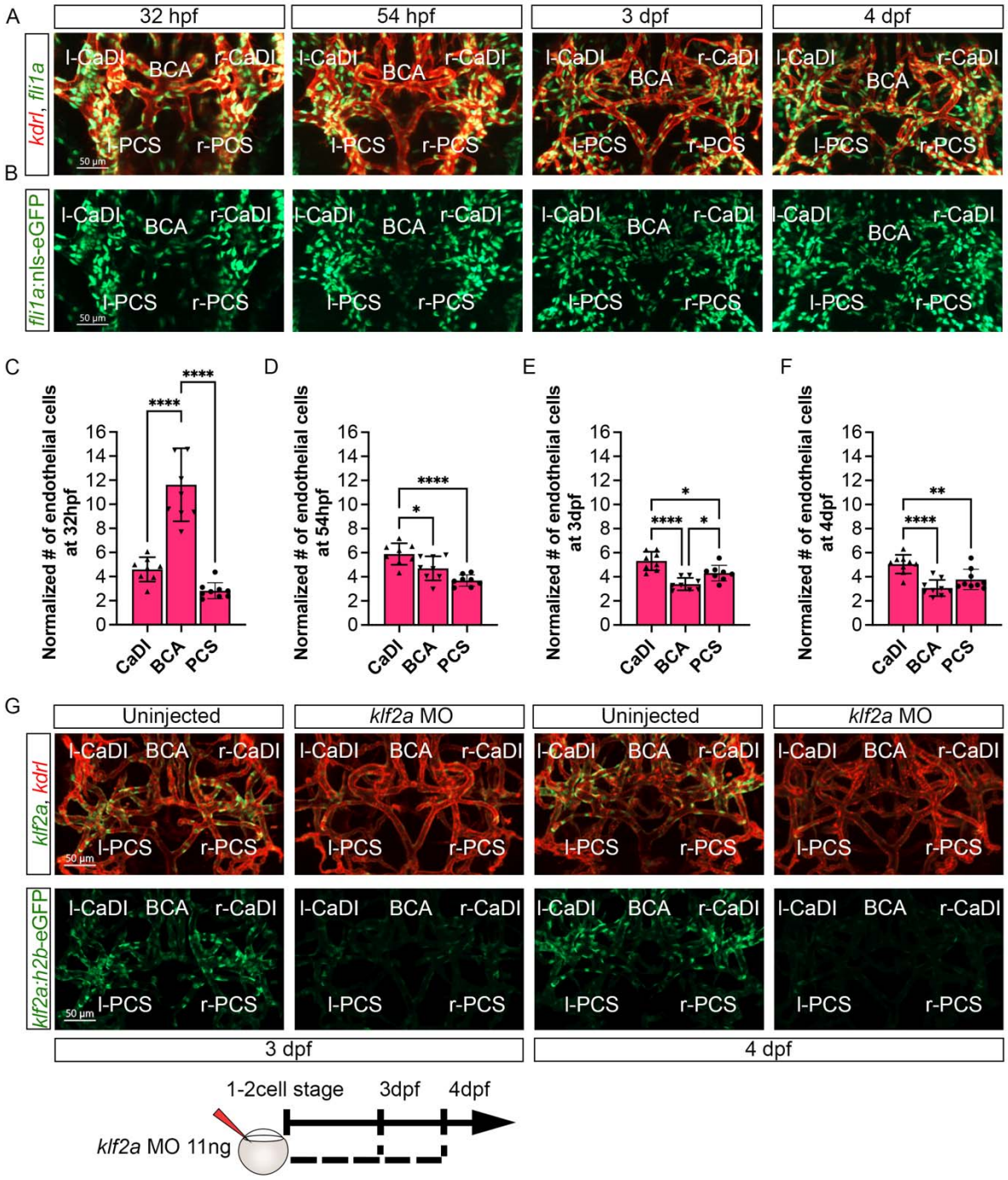
A
32 hpf
54 hpf
3 dpf
4 dpf
kdrl, fli1a
l-CaDI
BCA
r-CaDI
l-PCS
r-PCS
50 µm
B
fli1a:nls-eGFP
C
D
E
F
Normalized # of endothelial cells at 32hpf
Normalized # of endothelial cells at 54hpf
Normalized # of endothelial cells at 3dpf
Normalized # of endothelial cells at 4dpf
CaDI
BCA
PCS
G
Uninjected
klf2a MO
klf2a, kdrl
klf2a:h2b-eGFP
3 dpf
4 dpf
1-2cell stage
3dpf
4dpf
klf2a MO 11ng
H
3 dpf uninjected
3 dpf klf2a MO 11 ng
Average intensity of klf2a:h2b-gfp
I
4 dpf uninjected
4 dpf klf2a MO 11 ng
J
Pearson correlation
Klf2+
Acta2+
r = 0.974
Normalized # of klf2+ cells at 3dpf
Normalized # of acta2+ cells at 3dpf

Figure S3. Number of endothelial cells (ECs) in circle of Willis (CoW) arteries does not increase during *klf2a* activation

(A-B) Confocal live images of Tg(*fli1:nls-gfp*, *kdrl:ras-mcherry*)$^{y7/s896}$ in CoW arteries of zebrafish brain at 32 hour post fertilization (hpf), 54 hpf, 3 day post fertilization (dpf), and 4 dpf. Red channel represents *kdrl:ras-mcherry* and Green channel represents *fli1:nls-gfp*. Scale bar = 50 μm

(C-F) Number of ECs per 100 μm vessel length on caudal division of internal carotid arteries (CaDI), basal communicating artery (BCA), and posterior communicating segments (PCS) at 32 hpf (n=9, 1 independent experiment) (C), 54 hpf (n=8, 1 independent experiment) (D), 3 dpf (n=8, 1 independent experiment) (E), and 4 dpf (n=9, 1 independent experiment) (F), ordinary one-way ANOVA analyses with Tukey's multiple comparisons, represented with mean ± SD, * p≤0.05, *** p≤0.001, **** p≤0.0001

(G) Confocal live images of Tg(*klf2a:h2b-gfp*, *kdrl:ras-mcherry*)$^{ig11/s896}$ in CoW arteries of zebrafish brain at 3 and 4 dpf in uninjected control and embryos injected with 11 ng of *klf2a* morpholino (MO). Red channel represents *kdrl:ras-mcherry* and Green channel represents *klf2a:h2b-gfp*. Scale bar = 50 μm

(H) Average intensity of *klf2a:h2b-gfp* in CaDI, BCA, and PCS at 3 dpf in uninjected control (n=3, 1 independent experiment) and embryos injected with 11 ng of *klf2a* MO (n=3, 1 independent experiment), two-tailed Mann–Whitney test on each vessel's comparison, represented with mean ± SD, * p≤0.05, *** p≤0.001, **** p≤0.0001

(I) Average intensity of *klf2a:h2b-gfp* in CaDI, BCA, and PCS at 4 dpf in uninjected control (n=3, 1 independent experiment) and embryos injected with 11 ng of *klf2a* MO (n=3, 1 independent experiment), two-tailed Mann–Whitney test on each vessel's comparison, represented with mean ± SD, * p≤0.05, **** p≤0.0001

(J) Linear regression with normalized # *klf2a*+ cells at 3 dpf (left y-axis) and normalized # *acta2*+ cells (right y-axis) with the different CoW arteries (CaDI, BCA and PCS, x-axis), and Pearson correlation coefficient (r) is provided, indicating the degree of linear relationship between two variables.

Abbreviations: hpf: hour post fertilization, dpf: day post fertilization, l-CaDI: left caudal division of internal carotid artery, r-CaDI: right caudal division of internal carotid artery, BCA: basal communicating artery, l-PCS: left posterior communicating segment, r-PCS: right posterior communicating segment

Reference

Abello, J., Raghavan, S., Yien, Y. Y., & Stratman, A. N. (2022). Peristaltic pumps adapted for laminar flow experiments enhance in vitro modeling of vascular cell behavior. *J Biol Chem, 298*(10), 102404. doi:10.1016/j.jbc.2022.102404

Aguilar-Pineda, J. A., Vera-Lopez, K. J., Shrivastava, P., Chavez-Fumagalli, M. A., Nieto-Montesinos, R., Alvarez-Fernandez, K. L., . . . Lino Cardenas, C. L. (2021). Vascular smooth muscle cell dysfunction contribute to neuroinflammation and Tau hyperphosphorylation in Alzheimer disease. *iScience, 24*(9), 102993. doi:10.1016/j.isci.2021.102993

Albinsson, S., Nordstrom, I., & Hellstrand, P. (2004). Stretch of the vascular wall induces smooth muscle differentiation by promoting actin polymerization. *J Biol Chem, 279*(33), 34849-34855. doi:10.1074/jbc.M403370200

Ando, K., Fukuhara, S., Izumi, N., Nakajima, H., Fukui, H., Kelsh, R. N., & Mochizuki, N. (2016). Clarification of mural cell coverage of vascular endothelial cells by live imaging of zebrafish. *Development, 143*(8), 1328-1339. doi:10.1242/dev.132654

Ando, K., Shih, Y. H., Ebarasi, L., Grosse, A., Portman, D., Chiba, A., . . . Lawson, N. D. (2021). Conserved and context-dependent roles for pdgfrb signaling during zebrafish vascular mural cell development. *Dev Biol, 479*, 11-22. doi:10.1016/j.ydbio.2021.06.010

Ando, K., Tong, L., Peng, D., Vazquez-Liebanas, E., Chiyoda, H., He, L., . . . Betsholtz, C. (2022). KCNJ8/ABCC9-containing K-ATP channel modulates brain vascular smooth muscle development and neurovascular coupling. *Dev Cell, 57*(11), 1383-1399 e1387. doi:10.1016/j.devcel.2022.04.019

Ando, K., Wang, W., Peng, D., Chiba, A., Lagendijk, A. K., Barske, L., . . . Betsholtz, C. (2019). Peri-arterial specification of vascular mural cells from naive mesenchyme requires Notch signaling. *Development, 146*(2). doi:10.1242/dev.165589

ANSYS. (2014). ANSYS Innovation Courses: 3D bifurcating artery. Retrieved from https://courses.ansys.com/index.php/courses/fluent-3d-bifurcating-artery/

Bahrami, N., & Childs, S. J. (2020). Development of vascular regulation in the zebrafish embryo. *Development, 147*(10). doi:10.1242/dev.183061

Barak, T., Ristori, E., Ercan-Sencicek, A. G., Miyagishima, D. F., Nelson-Williams, C., Dong, W., . . . Gunel, M. (2021). PPIL4 is essential for brain angiogenesis and implicated in intracranial aneurysms in humans. *Nat Med, 27*(12), 2165-2175. doi:10.1038/s41591-021-01572-7

Basatemur, G. L., Jorgensen, H. F., Clarke, M. C. H., Bennett, M. R., & Mallat, Z. (2019). Vascular smooth muscle cells in atherosclerosis. *Nat Rev Cardiol, 16*(12), 727-744. doi:10.1038/s41569-019-0227-9

Campbell, B. C. V., De Silva, D. A., Macleod, M. R., Coutts, S. B., Schwamm, L. H., Davis, S. M., & Donnan, G. A. (2019). Ischaemic stroke. *Nat Rev Dis Primers, 5*(1), 70. doi:10.1038/s41572-019-0118-8

Cao, W., Zhang, D., Li, Q., Liu, Y., Jing, S., Cui, J., . . . Yu, B. (2017). Biomechanical Stretch Induces Inflammation, Proliferation, and Migration by Activating NFAT5 in Arterial Smooth Muscle Cells. *Inflammation, 40*(6), 2129-2136. doi:10.1007/s10753-017-0653-y

Chandra, S. M., Razavi, H., Kim, J., Agrawal, R., Kundu, R. K., de Jesus Perez, V., . . . Chun, H. J. (2011). Disruption of the apelin-APJ system worsens hypoxia-induced pulmonary hypertension. *Arterioscler Thromb Vasc Biol, 31*(4), 814-820. doi:10.1161/ATVBAHA.110.219980

Chen, X., Gays, D., Milia, C., & Santoro, M. M. (2017). Cilia Control Vascular Mural Cell Recruitment in Vertebrates. *Cell Rep, 18*(4), 1033-1047. doi:10.1016/j.celrep.2016.12.044

Chen, Z., Qin, H., Liu, J., Wu, B., Cheng, Z., Jiang, Y., . . . Wang, Y. (2019). Characteristics of Wall Shear Stress and Pressure of Intracranial Atherosclerosis Analyzed by a Computational Fluid Dynamics Model: A Pilot Study. *Front Neurol, 10*, 1372. doi:10.3389/fneur.2019.01372

Chi, N. C., Shaw, R. M., De Val, S., Kang, G., Jan, L. Y., Black, B. L., & Stainier, D. Y. (2008). Foxn4 directly regulates tbx2b expression and atrioventricular canal formation. *Genes Dev, 22*(6), 734-739. doi:10.1101/gad.1629408

Chou, E. L., Lino Cardenas, C. L., Chaffin, M., Arduini, A. D., Juric, D., Stone, J. R., . . . Lindsay, M. E. (2022). Vascular smooth muscle cell phenotype switching in carotid atherosclerosis. *JVS Vasc Sci, 3*, 41-47. doi:10.1016/j.jvssci.2021.11.002

Colijn, S., Nambara, M., & Stratman, A. N. (2023). Identification of overlapping and distinct mural cell populations during early embryonic development. *bioRxiv*, 2023.2004.2003.535476. doi:10.1101/2023.04.03.535476

Cross, L. M., Cook, M. A., Lin, S., Chen, J. N., & Rubinstein, A. L. (2003). Rapid analysis of angiogenesis drugs in a live fluorescent zebrafish assay. *Arterioscler Thromb Vasc Biol, 23*(5), 911-912. doi:10.1161/01.ATV.0000068685.72914.7E

Crouch, E. E., Bhaduri, A., Andrews, M. G., Cebrian-Silla, A., Diafos, L. N., Birrueta, J. O., . . . Huang, E. J. (2022). Ensembles of endothelial and mural cells promote angiogenesis in prenatal human brain. *Cell, 185*(20), 3753-3769 e3718. doi:10.1016/j.cell.2022.09.004

Dekker, R. J., van Soest, S., Fontijn, R. D., Salamanca, S., de Groot, P. G., VanBavel, E., . . . Horrevoets, A. J. (2002). Prolonged fluid shear stress induces a distinct set of endothelial cell genes, most specifically lung Kruppel-like factor (KLF2). *Blood, 100*(5), 1689-1698. doi:10.1182/blood-2002-01-0046

Donadon, M., & Santoro, M. M. (2021). The origin and mechanisms of smooth muscle cell development in vertebrates. *Development, 148*(7). doi:ARTN dev197384

10.1242/dev.197384

Duchemin, A. L., Vignes, H., & Vermot, J. (2019). Mechanically activated piezo channels modulate outflow tract valve development through the Yap1 and Klf2-Notch signaling axis. *Elife, 8*. doi:10.7554/eLife.44706

Fernandes, M. C., Sousa, L. C., de Castro, C. F., da Palma, J. M. L. M., António, C. C., & Pinto, S. I. S. (2022). Implementation and Comparison of Non-Newtonian Viscosity Models in Hemodynamic Simulations of Patient Coronary Arteries. In *Theoretical Analyses, Computations, and Experiments of Multiscale Materials: A Tribute to Francesco dell'Isola* (pp. 403-428): Springer.

Fontana, F., Haack, T., Reichenbach, M., Knaus, P., Puceat, M., & Abdelilah-Seyfried, S. (2020). Antagonistic Activities of Vegfr3/Flt4 and Notch1b Fine-tune Mechanosensitive Signaling during Zebrafish Cardiac Valvulogenesis. *Cell Rep, 32*(2), 107883. doi:10.1016/j.celrep.2020.107883

Fox, B. M., Dorschel, K. B., Lawton, M. T., & Wanebo, J. E. (2021). Pathophysiology of Vascular Stenosis and Remodeling in Moyamoya Disease. *Front Neurol, 12*, 661578. doi:10.3389/fneur.2021.661578

Frosen, J., & Joutel, A. (2018). Smooth muscle cells of intracranial vessels: from development to disease. *Cardiovasc Res, 114*(4), 501-512. doi:10.1093/cvr/cvy002

Fujita, M., Cha, Y. R., Pham, V. N., Sakurai, A., Roman, B. L., Gutkind, J. S., & Weinstein, B. M. (2011). Assembly and patterning of the vascular network of the vertebrate hindbrain. *Development, 138*(9), 1705-1715. doi:10.1242/dev.058776

Gierten, J., Pylatiuk, C., Hammouda, O. T., Schock, C., Stegmaier, J., Wittbrodt, J., . . . Loosli, F. (2020). Automated high-throughput heartbeat quantification in medaka and zebrafish embryos under physiological conditions. *Sci Rep, 10*(1), 2046. doi:10.1038/s41598-020-58563-w

Goddard, L. M., Duchemin, A. L., Ramalingan, H., Wu, B., Chen, M., Bamezai, S., . . . Kahn, M. L. (2017). Hemodynamic Forces Sculpt Developing Heart Valves through a KLF2-WNT9B Paracrine Signaling Axis. *Dev Cell, 43*(3), 274-289 e275. doi:10.1016/j.devcel.2017.09.023

880 Goldschmidt, M. E., McLeod, K. J., & Taylor, W. R. (2001). Integrin-mediated mechanotransduction in vascular smooth muscle cells: frequency and force response characteristics. *Circ Res, 88*(7), 674-680. doi:10.1161/hh0701.089749

Gray, K. M., & Stroka, K. M. (2017). Vascular endothelial cell mechanosensing: New insights gained from biomimetic microfluidic models. *Semin Cell Dev Biol, 71*, 106-117.
885 doi:10.1016/j.semcdb.2017.06.002

Griffith, C. M., Huang, S. A., Cho, C., Khare, T. M., Rich, M., Lee, G. H., . . . Polacheck, W. J. (2020). Microfluidics for the study of mechanotransduction. *J Phys D Appl Phys, 53*(22). doi:10.1088/1361-6463/ab78d4

Haga, J. H., Li, Y. S., & Chien, S. (2007). Molecular basis of the effects of mechanical stretch on vascular
890 smooth muscle cells. *J Biomech, 40*(5), 947-960. doi:10.1016/j.jbiomech.2006.04.011

Heckel, E., Boselli, F., Roth, S., Krudewig, A., Belting, H. G., Charvin, G., & Vermot, J. (2015). Oscillatory Flow Modulates Mechanosensitive klf2a Expression through trpv4 and trpp2 during Heart Valve Development. *Curr Biol, 25*(10), 1354-1361. doi:10.1016/j.cub.2015.03.038

Hill, R. A., Tong, L., Yuan, P., Murikinati, S., Gupta, S., & Grutzendler, J. (2015). Regional Blood Flow in the
895 Normal and Ischemic Brain Is Controlled by Arteriolar Smooth Muscle Cell Contractility and Not by Capillary Pericytes. *Neuron, 87*(1), 95-110. doi:10.1016/j.neuron.2015.06.001

Hogan, B. M., Herpers, R., Witte, M., Helotera, H., Alitalo, K., Duckers, H. J., & Schulte-Merker, S. (2009). Vegfc/Flt4 signalling is suppressed by Dll4 in developing zebrafish intersegmental arteries. *Development, 136*(23), 4001-4009. doi:10.1242/dev.039990

900 Isogai, S., Horiguchi, M., & Weinstein, B. M. (2001). The vascular anatomy of the developing zebrafish: an atlas of embryonic and early larval development. *Dev Biol, 230*(2), 278-301. doi:10.1006/dbio.2000.9995

Kaplan, L., Chow, B. W., & Gu, C. (2020). Neuronal regulation of the blood-brain barrier and neurovascular coupling. *Nat Rev Neurosci, 21*(8), 416-432. doi:10.1038/s41583-020-0322-2

905 Kathuria, S., Gregg, L., Chen, J., & Gandhi, D. (2011). Normal cerebral arterial development and variations. *Semin Ultrasound CT MR, 32*(3), 242-251. doi:10.1053/j.sult.2011.02.002

Katritsis, D., Kaiktsis, L., Chaniotis, A., Pantos, J., Efstathopoulos, E. P., & Marmarelis, V. (2007). Wall shear stress: theoretical considerations and methods of measurement. *Prog Cardiovasc Dis, 49*(5), 307-329. doi:10.1016/j.pcad.2006.11.001

910 Lee, J. S., Yu, Q., Shin, J. T., Sebzda, E., Bertozzi, C., Chen, M., . . . Kahn, M. L. (2006). Klf2 is an essential regulator of vascular hemodynamic forces in vivo. *Dev Cell, 11*(6), 845-857. doi:10.1016/j.devcel.2006.09.006

Leung, D. Y., Glagov, S., & Mathews, M. B. (1976). Cyclic stretching stimulates synthesis of matrix components by arterial smooth muscle cells in vitro. *Science, 191*(4226), 475-477.
915 doi:10.1126/science.128820

Menshawi, K., Mohr, J. P., & Gutierrez, J. (2015). A Functional Perspective on the Embryology and Anatomy of the Cerebral Blood Supply. *J Stroke, 17*(2), 144-158. doi:10.5853/jos.2015.17.2.144

Milewicz, D. M., Kwartler, C. S., Papke, C. L., Regalado, E. S., Cao, J., & Reid, A. J. (2010). Genetic variants promoting smooth muscle cell proliferation can result in diffuse and diverse vascular diseases:
920 evidence for a hyperplastic vasculomyopathy. *Genet Med, 12*(4), 196-203. doi:10.1097/GIM.0b013e3181cdd687

Milewicz, D. M., Trybus, K. M., Guo, D. C., Sweeney, H. L., Regalado, E., Kamm, K., & Stull, J. T. (2017). Altered Smooth Muscle Cell Force Generation as a Driver of Thoracic Aortic Aneurysms and Dissections. *Arterioscler Thromb Vasc Biol, 37*(1), 26-34. doi:10.1161/ATVBAHA.116.303229

925 Mirabella, T., MacArthur, J. W., Cheng, D., Ozaki, C. K., Woo, Y. J., Yang, M., & Chen, C. S. (2017). 3D-printed vascular networks direct therapeutic angiogenesis in ischaemia. *Nat Biomed Eng, 1*. doi:10.1038/s41551-017-0083

Nicoli, S., Standley, C., Walker, P., Hurlstone, A., Fogarty, K. E., & Lawson, N. D. (2010). MicroRNA-mediated integration of haemodynamics and Vegf signalling during angiogenesis. *Nature, 464*(7292), 1196-1200. doi:10.1038/nature08889

Nowotarski, S. H., & Sánchez Alvarado, A. (2016). Widening perspectives on regenerative processes through growth. *npj Regenerative Medicine, 1*(1), 16015. doi:10.1038/npjregenmed.2016.15

Oka, M., Shimo, S., Ohno, N., Imai, H., Abekura, Y., Koseki, H., . . . Aoki, T. (2020). Dedifferentiation of smooth muscle cells in intracranial aneurysms and its potential contribution to the pathogenesis. *Sci Rep, 10*(1), 8330. doi:10.1038/s41598-020-65361-x

Page, D. M., Wittamer, V., Bertrand, J. Y., Lewis, K. L., Pratt, D. N., Delgado, N., . . . Traver, D. (2013). An evolutionarily conserved program of B-cell development and activation in zebrafish. *Blood, 122*(8), e1-11. doi:10.1182/blood-2012-12-471029

Parmar, K. M., Larman, H. B., Dai, G., Zhang, Y., Wang, E. T., Moorthy, S. N., . . . Garcia-Cardena, G. (2006). Integration of flow-dependent endothelial phenotypes by Kruppel-like factor 2. *J Clin Invest, 116*(1), 49-58. doi:10.1172/JCI24787

Poittevin, M., Lozeron, P., Hilal, R., Levy, B. I., Merkulova-Rainon, T., & Kubis, N. (2014). Smooth muscle cell phenotypic switching in stroke. *Transl Stroke Res, 5*(3), 377-384. doi:10.1007/s12975-013-0306-x

Quevedo, J., Vianna, M., Daroit, D., Born, A. G., Kuyven, C. R., Roesler, R., & Quillfeldt, J. A. (1998). L-type voltage-dependent calcium channel blocker nifedipine enhances memory retention when infused into the hippocampus. *Neurobiol Learn Mem, 69*(3), 320-325. doi:10.1006/nlme.1998.3822

Rasouli, S. J., El-Brolosy, M., Tsedeke, A. T., Bensimon-Brito, A., Ghanbari, P., Maischein, H. M., . . . Stainier, D. Y. (2018). The flow responsive transcription factor Klf2 is required for myocardial wall integrity by modulating Fgf signaling. *Elife, 7*. doi:10.7554/eLife.38889

Robin, Y. M., Penel, N., Perot, G., Neuville, A., Velasco, V., Ranchere-Vince, D., . . . Coindre, J. M. (2013). Transgelin is a novel marker of smooth muscle differentiation that improves diagnostic accuracy of leiomyosarcomas: a comparative immunohistochemical reappraisal of myogenic markers in 900 soft tissue tumors. *Mod Pathol, 26*(4), 502-510. doi:10.1038/modpathol.2012.192

Roman, B. L., Pham, V. N., Lawson, N. D., Kulik, M., Childs, S., Lekven, A. C., . . . Weinstein, B. M. (2002). Disruption of acvrl1 increases endothelial cell number in zebrafish cranial vessels. *Development, 129*(12), 3009-3019. doi:10.1242/dev.129.12.3009

Schröder, H., Moser, N., & Huggenberger, S. (2020). The Mouse Circle of Willis. In *Neuroanatomy of the Mouse: An Introduction* (pp. 333-340). Cham: Springer International Publishing.

Sehnert, A. J., Huq, A., Weinstein, B. M., Walker, C., Fishman, M., & Stainier, D. Y. (2002). Cardiac troponin T is essential in sarcomere assembly and cardiac contractility. *Nat Genet, 31*(1), 106-110. doi:10.1038/ng875

Sharif-Naeini, R., Folgering, J. H., Bichet, D., Duprat, F., Lauritzen, I., Arhatte, M., . . . Honore, E. (2009). Polycystin-1 and -2 dosage regulates pressure sensing. *Cell, 139*(3), 587-596. doi:10.1016/j.cell.2009.08.045

Steed, E., Faggianelli, N., Roth, S., Ramspacher, C., Concordet, J. P., & Vermot, J. (2016). klf2a couples mechanotransduction and zebrafish valve morphogenesis through fibronectin synthesis. *Nat Commun, 7*, 11646. doi:10.1038/ncomms11646

Stratman, A. N., Burns, M. C., Farrelly, O. M., Davis, A. E., Li, W., Pham, V. N., . . . Weinstein, B. M. (2020). Chemokine mediated signalling within arteries promotes vascular smooth muscle cell recruitment. *Commun Biol, 3*(1), 734. doi:10.1038/s42003-020-01462-7

Stratman, A. N., Pezoa, S. A., Farrelly, O. M., Castranova, D., Dye, L. E., 3rd, Butler, M. G., . . . Weinstein, B. M. (2017). Interactions between mural cells and endothelial cells stabilize the developing zebrafish dorsal aorta. *Development, 144*(1), 115-127. doi:10.1242/dev.143131

Stratman, A. N., & Weinstein, B. M. (2021). Assessment of Vascular Patterning in the Zebrafish. *Methods Mol Biol, 2206*, 205-222. doi:10.1007/978-1-0716-0916-3_15

Traver, D., Paw, B. H., Poss, K. D., Penberthy, W. T., Lin, S., & Zon, L. I. (2003). Transplantation and in vivo imaging of multilineage engraftment in zebrafish bloodless mutants. *Nat Immunol, 4*(12), 1238-1246. doi:10.1038/ni1007

Turczynska, K. M., Hellstrand, P., Sward, K., & Albinsson, S. (2013). Regulation of vascular smooth muscle mechanotransduction by microRNAs and L-type calcium channels. *Commun Integr Biol, 6*(1), e22278. doi:10.4161/cib.22278

Ulrich, F., Ma, L. H., Baker, R. G., & Torres-Vazquez, J. (2011). Neurovascular development in the embryonic zebrafish hindbrain. *Dev Biol, 357*(1), 134-151. doi:10.1016/j.ydbio.2011.06.037

Vila Cuenca, M., Cochrane, A., van den Hil, F. E., de Vries, A. A. F., Lesnik Oberstein, S. A. J., Mummery, C. L., & Orlova, V. V. (2021). Engineered 3D vessel-on-chip using hiPSC-derived endothelial- and vascular smooth muscle cells. *Stem Cell Reports, 16*(9), 2159-2168. doi:10.1016/j.stemcr.2021.08.003

Wang, Y., Cao, W., Cui, J., Yu, Y., Zhao, Y., Shi, J., . . . Liu, J. (2018). Arterial Wall Stress Induces Phenotypic Switching of Arterial Smooth Muscle Cells in Vascular Remodeling by Activating the YAP/TAZ Signaling Pathway. *Cell Physiol Biochem, 51*(2), 842-853. doi:10.1159/000495376

Watterston, C., Zeng, L., Onabadejo, A., & Childs, S. J. (2019). MicroRNA26 attenuates vascular smooth muscle maturation via endothelial BMP signalling. *PLoS Genet, 15*(5), e1008163. doi:10.1371/journal.pgen.1008163

Whitesell, T. R., Chrystal, P. W., Ryu, J. R., Munsie, N., Grosse, A., French, C. R., . . . Childs, S. J. (2019). foxc1 is required for embryonic head vascular smooth muscle differentiation in zebrafish. *Dev Biol, 453*(1), 34-47. doi:10.1016/j.ydbio.2019.06.005

Whitesell, T. R., Kennedy, R. M., Carter, A. D., Rollins, E. L., Georgijevic, S., Santoro, M. M., & Childs, S. J. (2014). An alpha-smooth muscle actin (acta2/alphasma) zebrafish transgenic line marking vascular mural cells and visceral smooth muscle cells. *PLoS One, 9*(3), e90590. doi:10.1371/journal.pone.0090590

Wilson, E., Sudhir, K., & Ives, H. E. (1995). Mechanical strain of rat vascular smooth muscle cells is sensed by specific extracellular matrix/integrin interactions. *J Clin Invest, 96*(5), 2364-2372. doi:10.1172/JCI118293

Wu, J., Bohanan, C. S., Neumann, J. C., & Lingrel, J. B. (2008). KLF2 transcription factor modulates blood vessel maturation through smooth muscle cell migration. *J Biol Chem, 283*(7), 3942-3950. doi:10.1074/jbc.M707882200

Zhong, H., Wu, X., Huang, H., Fan, Q., Zhu, Z., & Lin, S. (2006). Vertebrate MAX-1 is required for vascular patterning in zebrafish. *Proc Natl Acad Sci U S A, 103*(45), 16800-16805. doi:10.1073/pnas.0603959103